© 2021. Published by The Company of Biologists Ltd | Development (2021) 148, dev189191. doi:10.1242/dev.189191

STEM CELLS AND REGENERATION

RESEARCH ARTICLE

Hes1 overexpression leads to expansion of embryonic neural stem cell pool and stem cell reservoir in the postnatal brain

Toshiyuki Ohtsuka[1,2,3,*] and Ryoichiro Kageyama[1,2,3,4]

ABSTRACT

Neural stem cells (NSCs) gradually alter their characteristics during mammalian neocortical development, resulting in the production of various neurons and glial cells, and remain in the postnatal brain as a source of adult neurogenesis. Notch-Hes signaling is a key regulator of stem cell properties in the developing and postnatal brain, and Hes1 is a major effector that strongly inhibits neuronal differentiation and maintains NSCs. To manipulate Hes1 expression levels in NSCs, we generated transgenic (Tg) mice using the Tet-On system. In Hes1-overexpressing Tg mice, NSCs were maintained in both embryonic and postnatal brains, and generation of later-born neurons was prolonged until later stages in the Tg neocortex. Hes1 overexpression inhibited the production of $Tbr2^+$ intermediate progenitor cells but instead promoted the generation of basal radial glia-like cells in the subventricular zone (SVZ) at late embryonic stages. Furthermore, Hes1-overexpressing Tg mice exhibited the expansion of NSCs and enhanced neurogenesis in the SVZ of adult brain. These results indicate that Hes1 overexpression expanded the embryonic NSC pool and led to the expansion of the NSC reservoir in the postnatal and adult brain.

KEY WORDS: Neural stem cell, Neocortical development, Neurogenesis, Notch, Hes1, Mouse

INTRODUCTION

At early stages of mammalian brain development, neuroepithelial cells, a primary form of neural stem cells (NSCs), proliferate to expand the NSC pool by repeated symmetric divisions, and the neural tube expands to form brain vesicles. Subsequently, neuroepithelial cells start neurogenesis and transform into radial glial cells (RGCs), another form of NSC. During the neurogenic period, RGCs asymmetrically divide in the innermost layer of the neural tube, termed the ventricular zone (VZ). One daughter cell remains as an NSC, and the other differentiates into a neuron or neuronal precursor cell such as an intermediate progenitor cell (IPC). Thus, brain vesicles/ventricles and the VZ enlarge during the symmetric proliferative division mode of NSCs but stop expanding once most NSCs shift to the asymmetric neurogenic division mode, because asymmetric divisions no longer contribute to an increase in NSC numbers (Takahashi et al., 1995, 1999). During the neurogenic period, NSCs in neocortical regions sequentially give rise to deep layer neurons and then superficial layer neurons. At late embryonic stages, NSCs finish neurogenesis and shift to the gliogenic phase, in which astrocytes are mainly produced. Only a subset of NSCs remain in specific regions of the postnatal and adult brain as astrocyte-like cells that retain stemness. These NSC populations in the two major neurogenic niches in the adult brain – the subventricular zone (SVZ) of the rostral part of lateral ventricles and the dentate gyrus of the hippocampus – continue neurogenesis. Indeed, adult neurogenesis is important for the maintenance of cognitive functions such as spatial memory (Imayoshi et al., 2008) and innate olfactory responses (Sakamoto et al., 2011). However, the mechanisms underpinning the sorting and maintenance of a fraction of embryonic NSCs as adult NSCs, and how the number of NSCs in the adult brain is governed, remain elusive.

The Hes family of basic helix-loop-helix (bHLH) transcriptional repressors (Hes1, Hes3 and Hes5) function downstream of Notch signaling (Kageyama and Ohtsuka, 1999), strongly inhibit neuronal differentiation, and maintain NSCs in the developing mammalian brain by repressing the proneural (neurogenic) bHLH factors such as Ascl1 and Neurog1/2 (Ishibashi et al., 1994; Ohtsuka et al., 1999, 2001; Hirata et al., 2000; Hatakeyama et al., 2004). Hes1 single mutant mice demonstrate severe phenotypes caused by accelerated neuronal differentiation, whereas Hes3 or Hes5 mutant mice exhibit only mild phenotypes owing to compensation by upregulated Hes1 (Ishibashi et al., 1995; Ohtsuka et al., 1999; Cau et al., 2000; Hirata et al., 2001). It is thus likely that Hes1 is an essential and dominant factor among the Hes family of repressors that maintains NSCs in an undifferentiated state.

It has been reported that certain alterations occurred in the cellular composition of the developing neocortex during mammalian brain evolution; the secondary germinal layer known as the outer subventricular zone (OSVZ) containing basal RGCs (bRGCs) emerged and distinctively developed during the course of evolution from lissencephalic to gyrencephalic mammals (Hansen et al., 2010; Molnár et al., 2011; Wang et al., 2011; Lui et al., 2011; Reillo et al., 2011; Hevner and Haydar, 2012; LaMonica et al., 2012). These bRGCs behave as an additional NSC pool that continues proliferation and neurogenesis during mid to late embryonic stages and contributes to the expansion of neuronal numbers and cortical surface areas in gyrencephalic mammals. bRGCs have similar molecular characteristics as those of apical RGCs (aRGCs); they are positive for Hes1, Pax6 and Sox2 (markers of NSCs), and negative for Tbr2 (also known as Eomes), a marker of IPCs.

To address how the manipulation of Hes1 expression in NSCs impacts morphology and cell composition of the developing and postnatal brain, we generated transgenic (Tg) mice in which Hes1 expression is controllable by using the Tet-On system. Here, we confirmed that Hes1 overexpression led to maintenance and expansion of NSCs in the embryonic brain, and found that later-born neurons (superficial layer neurons) were slowly produced and neurogenesis was prolonged, whereas gliogenesis was

[1]Institute for Frontier Life and Medical Sciences, Kyoto University, 53 Kawahara-cho, Shogoin, Sakyo-ku, Kyoto 606-8507, Japan. [2]Graduate School of Medicine, Kyoto University, Kyoto 606-8501, Japan. [3]Graduate School of Biostudies, Kyoto University, Kyoto 606-8501, Japan. [4]Institute for Integrated Cell-Material Sciences (iCeMS), Kyoto University, Kyoto 606-8501, Japan.

*Author for correspondence (tohtsuka@infront.kyoto-u.ac.jp)

T.O., 0000-0001-6045-1012

Handling Editor: François Guillemot
Received 25 March 2020; Accepted 14 January 2021

Development (2021) 148, dev189191. doi:10.1242/dev.189191

paradoxically accelerated in the Tg cortex. Notably, we observed that bRGC-like cells were increased in the SVZ of Tg cortex at late embryonic stages, suggesting their contribution to the prolonged neurogenesis observed in the Tg cortex. Furthermore, we observed that the number of slowly-dividing Pax6^{+} cells was increased and neurogenesis was enhanced, particularly when Hes1 expression was downregulated, in the dorsal and dorsolateral SVZ of the adult Tg brain, implicating an expanded reservoir of NSCs in the Hes1-overexpressing Tg brain.

RESULTS

Lateral ventricles and VZ were enlarged in Hes1-overexpressing Tg embryos

We generated and crossed two Tg mouse lines (Fig. 1A); the reverse tetracycline-controlled transactivator (rtTA) is driven by the promoter and second intron of the nestin gene and expressed in NSCs and neural progenitors (*pNestin-rtTA* Tg) and, in the presence of doxycycline (Dox), rtTA binds to the tetracycline (Tet)-responsive element (TRE) and bi-directionally activates expression of *Hes1* and *d2EGFP*, a destabilized variant of enhanced green fluorescent protein (EGFP) with a half-life of ∼2 h (*TRE-Hes1/d2EGFP* Tg). Thus, Hes1 and d2EGFP were overexpressed in NSCs and neural progenitors in double Tg mice when Dox was administered. GFP expression was detected in the brain, spinal cord, eyes and parts of the skin of these Hes1-overexpressing Tg mice (Fig. 1B; Fig. S1A,B). The size of embryonic and postnatal brains of Tg mice was slightly smaller than that of wild-type (WT) mice (Fig. S1B,C), and the difference in body size between Tg and WT pups became larger during postnatal stages (Fig. S1D,E). Immunohistochemistry on coronal brain sections using antibodies against GFP and Hes1 revealed that expression of d2EGFP

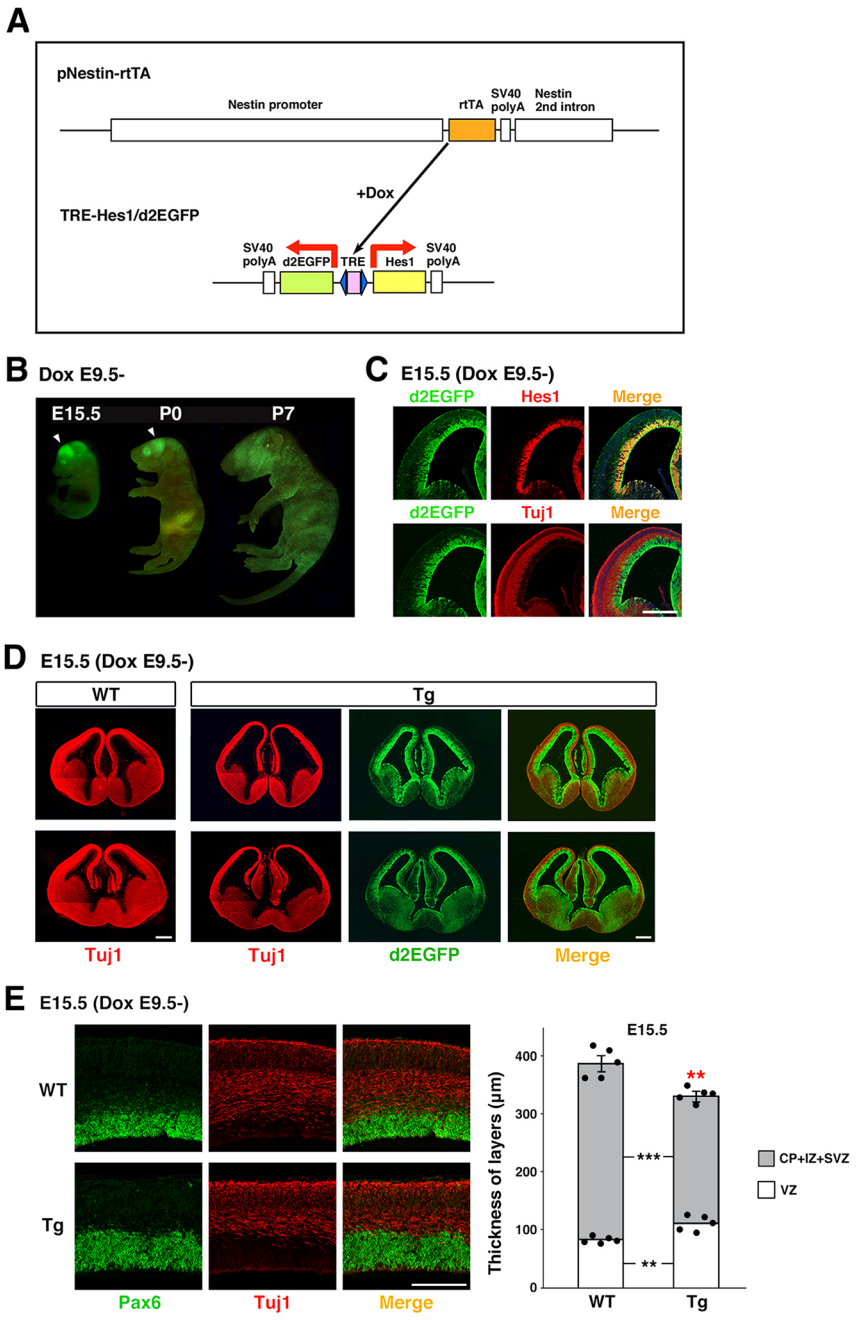

Fig. 1. Generation of Hes1-overexpressing transgenic mice. (A) Structure of *pNestin-rtTA* and *TRE-Hes1/d2EGFP* transgenes. Mice generated by crossing both transgenic (Tg) lines bidirectionally express Hes1 and the fluorescent reporter d2EGFP in nestin-expressing cells including NSCs in the presence of doxycycline (Dox). (B) GFP expression (green) in Hes1-overexpressing Tg mice at E15.5, P0 and P7. Dox was administered from E9.5. Arrowheads indicate GFP expression in the telencephalon. (C) Coronal sections of the telencephalon of E15.5 Tg embryo double-stained using anti-GFP (green) and anti-Hes1 or anti-Tuj1 (red) antibodies. (D) Immunostaining with anti-Tuj1 (red) and anti-GFP (green) antibodies on coronal sections of the telencephalon of wild-type (WT) and Tg embryos at E15.5. (E) Higher magnification views of neocortical areas of WT and Tg embryos stained with anti-Pax6 (green) and anti-Tuj1 (red) antibodies. Quantification (right) shows the thicknesses of the VZ and upper layers (CP+IZ+SVZ) in the neocortical regions of WT and Tg brains at E15.5. Data are mean±s.e.m. (n=5). **P<0.01, ***P<0.001 (unpaired two-tailed Student's t-test). Scale bars: 500 µm in C, D; 200 µm in E.

Development (2021) 148, dev189191. doi:10.1242/dev.189191

was mostly restricted to the VZ, and high levels of Hes1 were co-expressed in GFP$^+$ cells (Fig. 1C). Expression of d2EGFP and high levels of Hes1 were detected by 2 days after the start of continuous Dox (1.0 mg/ml in drinking water) administration to pregnant mice. Notably, the lateral ventricles were remarkably enlarged and the VZ (demarcated by immunostaining for Pax6, a marker of NSCs in developmental stages) was thicker in the Tg brain (Fig. 1D,E). In contrast, outer neuronal layers (indicated by immunostaining for the neuronal marker Tuj1), including the cortical plate (CP), intermediate zone (IZ) and SVZ, and the total cortical thickness were thinner compared with the WT brain. The ventral telencephalon including the ganglionic eminences was also thinner and hypoplastic in the Tg brain.

NSCs were maintained and neuronal differentiation was inhibited in Hes1-overexpressing Tg embryos

In Hes1-overexpressing Tg embryos, the VZ became thicker and expanded in tangential directions, whereas outer layers (including CP, IZ, and SVZ) and the total cortical thickness became thinner compared with the WT brain after embryonic day (E) 15.5 (Fig. 2A, B), suggesting that the NSC population was expanded and neurogenesis was suppressed by Hes1 overexpression. The length of ventricular surface of the dorsolateral telencephalon, measured on the coronal section, was markedly longer in the Tg brain, although the length of cortical surface was comparable with that of the WT brain (Fig. 2A,B). The expression of d2EGFP and Hes1 essentially overlapped with Pax6 staining. Notably, a higher number of Pax6$^+$ cells remained in the VZ of the dorsolateral telencephalon (neocortical regions) of Tg mice until postnatal stages, whereas their number was substantially attenuated by postnatal day (P) 0 in the WT brain (Fig. 2A,B). It appeared that Pax6 expression was enhanced in some ventricular cells in the ganglionic eminences. It is possible that overexpression of Hes1 ectopically induced Pax6 expression in neural progenitors in the ventral telencephalon. Quantitative real-time RT-PCR revealed that Hes1 expression levels in the dorsolateral telencephalon in the Tg brain were 60 times higher than those in the WT brain at E15.5 (Fig. 2C). High levels of Hes1 and d2EGFP expression persisted in the VZ and SVZ of the Tg brain at later developmental stages and even after birth (Fig. 2D).

We performed *in situ* hybridization on coronal brain sections at E13.5 and estimated expression levels of *Hes1* and the proneural (neurogenic) bHLH gene *Neurog2* that is repressed by Hes1. *Hes1* expression levels were upregulated but, in contrast, *Neurog2* expression levels were markedly downregulated in the VZ of the Tg brain (Fig. 2E). *Neurog2* expression levels were still lower at E17.5, and *Neurog2*-expressing cells were mainly distributed outside the VZ in the Tg brain at P0, whereas *Neurog2* expression was mostly restricted to the VZ in the WT cortex. Immunohistochemistry using antibodies against Neurog2 revealed a significant decrease in Neurog2 expression levels in the VZ of the Tg brain at P0 (Fig. 2F). The majority of Neurog2$^+$ cells were located outside the VZ, and Neurog2 expression was segregated from d2EGFP expression. These results indicated that overexpression of Hes1 inhibited neuronal differentiation and maintained NSCs in an undifferentiated state by repressing expression of proneural (neurogenic) genes such as *Neurog2*.

Hes1 overexpression suppressed NSC proliferation

It has been reported that overexpression of Hes1 suppressed cell proliferation, and Hes1 represses the expression of cell cycle-related genes such as cyclin D1 (*Ccnd1*), cyclin E2 (*Ccne2*) and *Gadd45g* (Baek et al., 2006; Shimojo et al., 2008). Thus, we analyzed the rate of cell proliferation by 5-bromo-2′-deoxyuridine (BrdU) incorporation experiments, in which BrdU was intraperitoneally administered to pregnant mice 30 min before sacrifice, and the numbers of BrdU$^+$ cells that were also positive for Pax6 or Tbr2, a marker of IPCs, most of which are located in the SVZ, were counted within a radial column of constant width (200 µm) in neocortical regions. We observed a decrease in the number of BrdU$^+$ cells at E15.5 (Fig. 3A) and a significant decline in the proportions of BrdU$^+$ cells of Pax6$^+$ cells in neocortical regions of Tg brain at E13.5 and E15.5 (Fig. S2A,C). We performed immunohistochemistry using antibodies against phospho-histone H3 (pH3), a marker of dividing cells in the M phase; and Ki67 (Mki67), a marker of cycling cells. We observed that the numbers of pH3$^+$ cells and Ki67$^+$ cells in Tg mice were slightly less at E13.5 but significantly lower at E15.5 compared with those in WT mice (Fig. 3B,C). We then estimated the cell cycle length of Pax6$^+$ NSCs and observed that both the length of S phase (Ts) and the total cell cycle length (Tc) were significantly elongated in the Tg brain compared with the WT brain at E15.5. This indicated that NSC proliferation was suppressed by Hes1 overexpression (Fig. 3D). Given that the VZ was expanded in tangential directions and neurogenesis was suppressed in the Tg brain, it was suggested that NSCs continued symmetric proliferative divisions until later embryonic stages. We thus analyzed the division mode of NSCs and observed that NSCs continued expansion of Pax6$^+$ cells by symmetric proliferative divisions in the Tg brain, whereas significantly more NSCs produced Tbr2$^+$ IPCs by asymmetric neurogenic divisions in the WT brain (Fig. 3E).

We next examined the expression levels of Ccnd1 in the Tg brain using antibodies against Ccnd1. At E13.5 and E15.5, expression levels of Ccnd1 and the number of Ccnd1$^+$ cells were markedly reduced in the VZ of neocortical regions of Tg brain compared with the WT brain (Fig. 3F). At E17.5, expression levels of Ccnd1 were still lower in the VZ of Tg brain than in the VZ of the WT brain, although many Ccnd1$^+$ cells were observed around the SVZ of the Tg brain. The reduced expression levels of Ccnd1 in the dorsolateral telencephalon of E15.5 Tg mice were confirmed by quantitative real-time RT-PCR (Fig. 3G). These results indicated that high levels of Hes1 expression maintained NSCs but inhibited cell proliferation, partly due to the downregulation of cell cycle-related genes including Ccnd1. We analyzed cell death using anti-cleaved-caspase 3 (Casp3) antibody and observed that cell death was not significantly enhanced in neocortical regions of the Tg brain at E13.5 and E15.5 (Fig. S3).

Switching from deep to superficial layer neurogenesis occurred earlier in the Tg cortex

We have previously found that the transition timing from deep to superficial layer neurogenesis shifted earlier in the developing neocortex of Hes5-overexpressing Tg mice (Bansod et al., 2017). Therefore, we examined whether the timing of neurogenesis was disturbed in the Hes1-overexpressing Tg cortex by immunohistochemical analysis using markers for layer-specific neurons such as Tbr1 (layer VI), Ctip2 (Bcl11b; layer V), and Cux1 (layers II-IV). We observed that the onset of generation of early-born neurons (Tbr1$^+$ layer VI neurons and Ctip2$^+$ layer V neurons) was roughly comparable in Tg and WT mice (Fig. S4A). We subsequently performed birth date analyses by pulse labeling of DNA synthesis using BrdU. BrdU was intraperitoneally administered to pregnant mice at E13.5 or E14.5, and the fates and locations of BrdU-incorporated cells, which were born during the period of BrdU exposure, were analyzed by immunohistochemistry at P14. Most BrdU$^+$ cells differentiated into neurons, migrated out of the VZ and settled in the cortical layers at P14 (Fig. 4A,B). In the dorsal part of the cortex, many cells that incorporated BrdU at

Development (2021) 148, dev189191. doi:10.1242/dev.189191

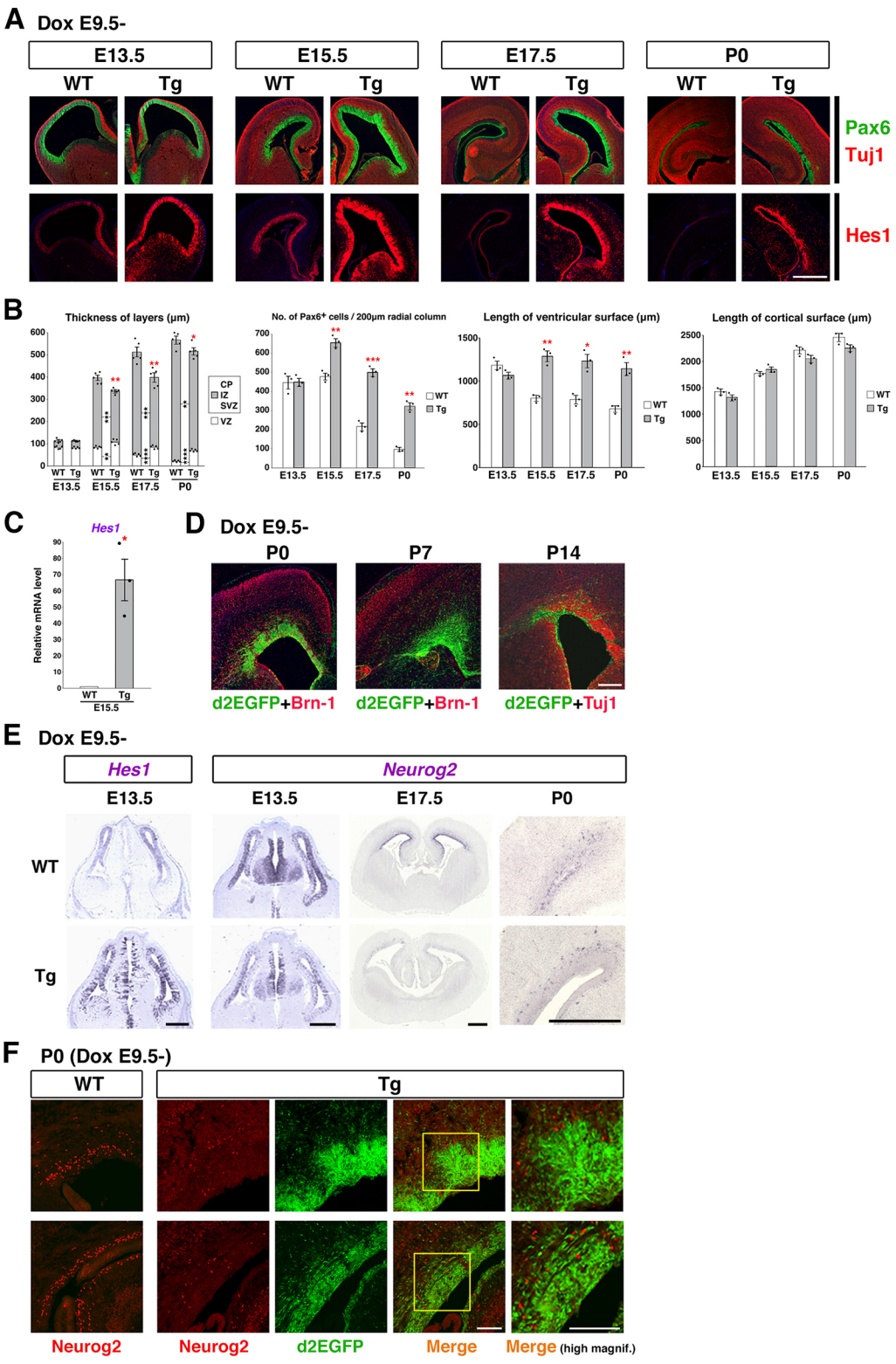

Fig. 2. Maintenance of NSCs and inhibition of neuronal differentiation. (A) Immunostaining with anti-Pax6 (green), anti-Tuj1 (red) (upper row), and anti-Hes1 (red) antibodies (bottom row) on coronal sections of neocortical regions of WT and Tg mice at various developmental stages. (B) Quantification showing the thicknesses of the VZ and upper layers (CP+IZ+SVZ), the numbers of Pax6^{+} cells within a radial column of 200 μm width, the length of ventricular surface and the length of cortical surface in the neocortical regions at the designated stages. (C) Real-time RT-PCR for *Hes1* using total RNAs prepared from the dorsolateral telencephalon (neocortical regions) of WT and Tg brains at E15.5. *Gapdh* was used as an internal control, and the values were normalized to that of the WT sample. (D) Immunostaining with anti-GFP (green) and anti-Brn-1 or anti-Tuj1 (red) antibodies on coronal sections of the brains of postnatal Tg mice at P0, P7 and P14. (E) *In situ* hybridization for *Hes1* or *Neurog2* was performed on coronal sections of WT and Tg brains at the indicated stages. (F) Immunostaining with anti-Neurog2 (red) and anti-GFP (green) antibodies on coronal sections of neocortical regions of WT and Tg mice at P0. The boxed areas in merged images are magnified in the rightmost panels. Data are mean±s.e.m. (n=3). *P<0.05, **P<0.01, ***P<0.001, ****P<0.0001 (unpaired two-tailed Student's t-test). Scale bars: 500 μm in A,D,E; 100 μm in F.

E13.5 were Ctip2^{+} and were located in the deep layers (layer V), and some cells were Cux1^{+} and were distributed in the superficial layers (layers II-IV). There was no significant difference in the distribution of BrdU^{+} cells between the WT and Tg cortices (Fig. 4A). Although many cells that incorporated BrdU at E14.5 remained Ctip2^{+} and were located in the deep layers in the WT cortex, the vast majority of BrdU^{+} cells were Cux1^{+} and were distributed in the superficial layers in the Tg cortex (Fig. 4B). These results indicated that the switching from deep to superficial layer neurogenesis occurred earlier in the Tg cortex compared with the WT cortex (Fig. 4C).

Production of superficial layer neurons was decelerated and prolonged

We further performed birth date analysis by double pulse labeling using BrdU and 5-iodo-2′-deoxyuridine (IdU) that were

Development (2021) 148, dev189191. doi:10.1242/dev.189191

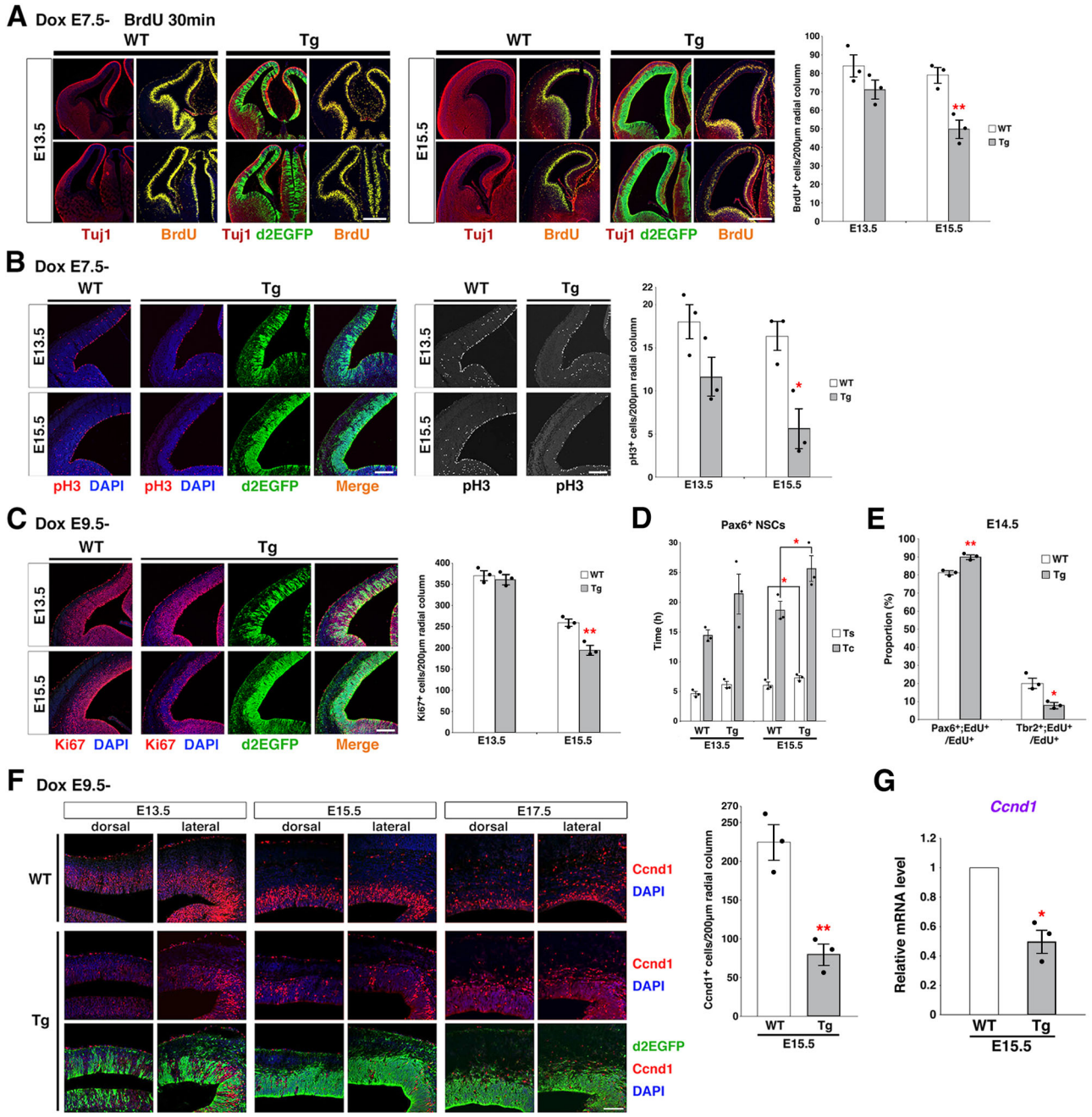

Fig. 3. Reduced cell proliferation in the VZ/SVZ of embryonic telencephalon. (A) Analysis of the cell proliferation rate by BrdU incorporation experiments. BrdU was injected intraperitoneally into pregnant mice 30 min before sacrifice. Coronal sections of the telencephalon of E13.5 and E15.5 embryos were immunostained using anti-Tuj1 (red), anti-BrdU (yellow) and anti-GFP (green) antibodies. Quantification (right) shows the numbers of BrdU+ cells within a radial column of 200 µm width. (B,C) Immunostaining with anti-pH3 (B) or anti-Ki67 (C) (red) antibody co-labeled with anti-GFP (green) antibody on coronal sections of neocortical regions at E13.5 (upper row) and E15.5 (bottom row). pH3 signals are shown in white on the right panels (grayscale). Graphs (right) show the numbers of pH3$^+$ (B) or Ki67$^+$ (C) cells within a radial column of 200 µm width. (D) Estimation of the cell cycle lengths of Pax6$^+$ NSCs in the neocortical regions at E13.5 and E15.5. Ts, length of S phase; Tc, total cell cycle length. (E) Analysis of the division mode of NSCs. The VZ cells (apical NSCs) were labeled by *in utero* electroporation with *pEF-mCherry* vector at E13.5, and EdU was injected intraperitoneally into pregnant mice 6 h after *in utero* electroporation. Proportions of Pax6$^+$;EdU$^+$/EdU$^+$ cells and Tbr2$^+$;EdU$^+$/EdU$^+$ cells were estimated 18 h after EdU administration at E14.5. (F) Double-labeling with anti-Ccnd1 (red) and anti-GFP (green) antibodies on coronal sections of the dorsal and lateral telencephalon at E13.5, E15.5 and E17.5. Quantification (right) shows the numbers of Ccnd1$^+$ cells within a radial column of 200 µm width. (G) Real-time RT-PCR for *Ccnd1* using total RNAs prepared from the dorsolateral telencephalon at E15.5. *Gapdh* was used as an internal control, and the values were normalized to that of the WT sample. DAPI (blue) represents nuclear staining. Data are mean±s.e.m. (n=3). *P<0.05, **P<0.01 (unpaired two-tailed Student's t-test). Scale bars: 500 µm in A; 200 µm in B,C; 100 µm in F.

intraperitoneally administered to pregnant mice at different embryonic stages. Cells that incorporated IdU at E13.5 were mostly located in the deep layers (layer V) and the deeper part of superficial layers (layer IV) in both WT and Tg mice at P14 (Fig. 4D,G). Cells that incorporated IdU or BrdU at E15.5 were located in the superficial layers (layers II-III) in both WT and Tg mice, although the number of IdU$^+$ or BrdU$^+$ cells was significantly less in the Tg cortex. In contrast, the number of cells that

Development (2021) 148, dev189191. doi:10.1242/dev.189191

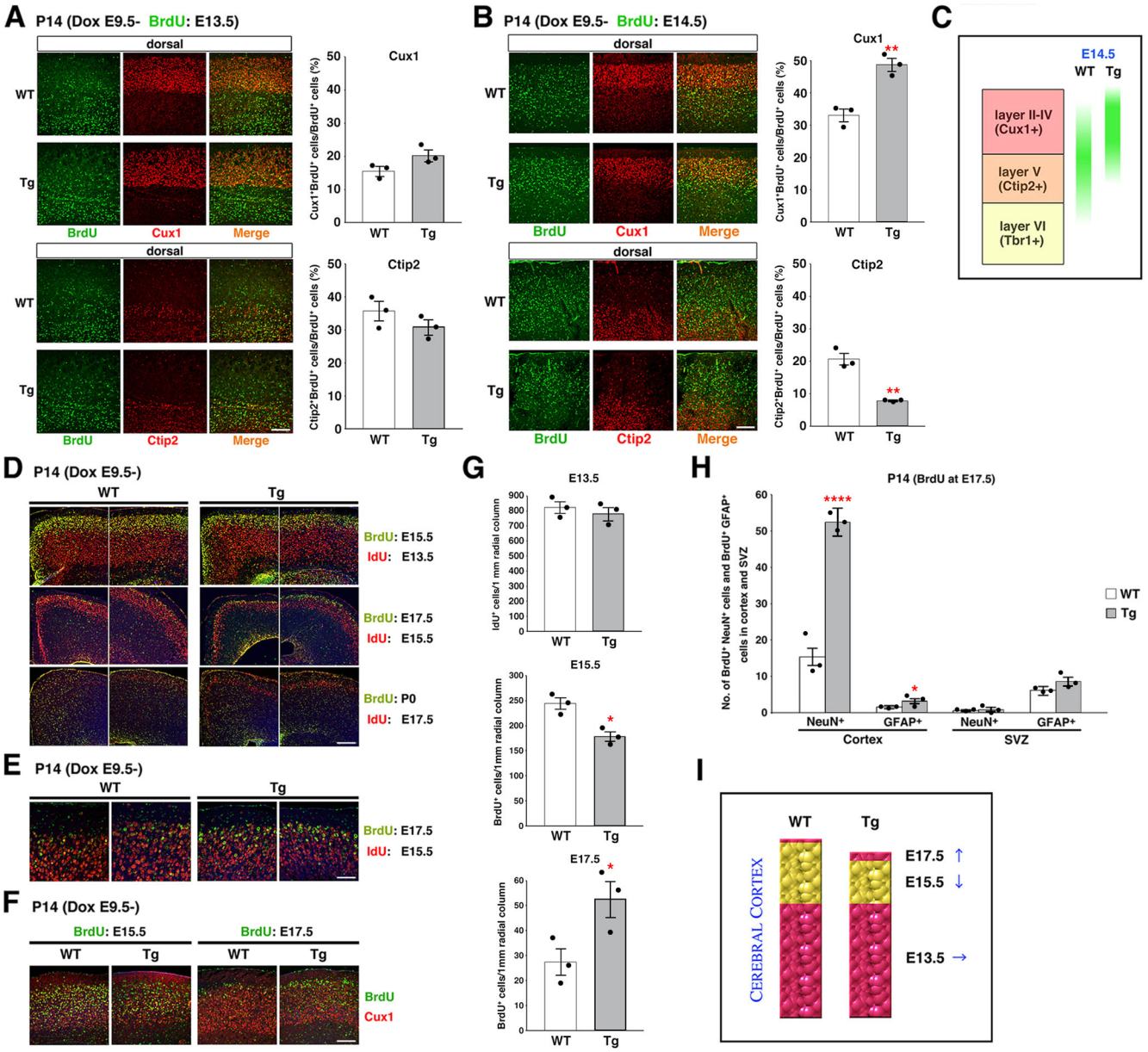

Fig. 4. Earlier switching from deep to superficial layer neurogenesis and prolonged generation of superficial layer neurons. (A,B) Birth date analysis by BrdU incorporation experiments. BrdU was injected intraperitoneally into pregnant mice at E13.5 (A) or E14.5 (B). Fates and location of cells that incorporated BrdU were analyzed by immunohistochemistry at P14. Coronal sections of the dorsal cortices were immunostained using anti-Cux1 or anti-Ctip2 (red) antibody co-labeled with anti-BrdU (green) antibody. Quantifications (right) show the proportions of $Cux1^+$ or $Ctip2^+$ cells of $BrdU^+$ cells. (C) Schematic showing the difference in distribution of cells that were born during the period of BrdU exposure at E14.5 in WT and Tg cortices. (D,E) Double pulse labeling using BrdU and IdU for the birth date analysis. BrdU and IdU were injected intraperitoneally into pregnant mice at the indicated stages. Cells that incorporated BrdU or IdU were detected by immunostaining on coronal sections of the dorsolateral cortex at P14. Higher magnification views of the labeling with IdU at E15.5 and BrdU at E17.5 are shown in E. (F) Double-labeling with anti-BrdU (green) and anti-Cux1 (red) antibodies on coronal sections of the dorsolateral cortex at P14. BrdU was injected at E15.5 (left) or E17.5 (right). (G) Graphs showing the numbers of IdU^+ (E13.5) or $BrdU^+$ (E15.5, E17.5) cells within a radial column of 1 mm width in the dorsolateral cortex. (H) Estimation of neurogenesis and gliogenesis at E17.5. BrdU was injected intraperitoneally into pregnant mice at E17.5, and the numbers of $BrdU^+$;$NeuN^+$ cells and $BrdU^+$;$GFAP^+$ cells were counted in the cortex and SVZ at P14. (I) Schematic demonstrating the comparison of numbers of cortical neurons generated at the examined stages. Data are mean±s.e.m. (n=3). *P<0.05, **P<0.01, ****P<0.0001 (unpaired two-tailed Student's t-test). Scale bars: 200 µm in A,B,F; 500 µm in D; 100 µm in E.

incorporated IdU or BrdU at E17.5 and settled in the most superficial layer of the cortex was increased in Tg mice compared with WT mice (Fig. 4D-G). To further characterize $BrdU^+$ cells, sections were stained with layer markers such as Ctip2 and Cux1. We confirmed that most of the cells that incorporated BrdU at E15.5 and E17.5 (mostly neurons generated at these stages) differentiated into $Cux1^+$ neurons (Fig. 4F). We analyzed the neuronal and glial fates of cells generated at E17.5 and found that a majority of cells that incorporated BrdU differentiated into $NeuN^+$ ($Rbfox3^+$) neurons in the Tg cortex at P14. In contrast, the number of $BrdU^+$;$GFAP^+$ cells was only slightly increased in the cortex and the SVZ (Fig. 4H). These results indicated that neurogenesis was decelerated around E15.5, but active neurogenesis persisted until later stages in the Tg cortex compared with the WT cortex, as

Development (2021) 148, dev189191. doi:10.1242/dev.189191

illustrated by the schematic in Fig. 4I. Thus, the timing of neurogenesis was disrupted by Hes1 overexpression, especially during later developmental stages.

However, the cortical layer structure was not significantly disorganized in the postnatal brain, although all layers were thinner in the Tg cortex than in the WT cortex (Fig. S4B). The cortical thickness is generally thinner in the Tg brain during embryonic stages, but the difference became less after postnatal stages, probably because mice with the severe phenotype could not survive and only those with the mild phenotype survived after postnatal stages.

Astrocytes were prematurely generated and diffusely distributed

As neurogenesis persisted until later stages in the Tg brain, we investigated whether the onset of gliogenesis was shifted in the Tg brain, using glial markers such as GFAP, a marker of astrocytes; Olig2, a marker of oligodendrocytes; and PDGFRα, a marker of oligodendrocyte precursor cells. We found that high GFAP signals were focally detected in the VZ of neocortical regions of Tg brain at P0 (Fig. 5A), whereas only faint GFAP expression was observed in the same regions of WT brain. This observation indicated that astrogenesis prematurely occurred in the Hes1-overexpressing Tg brain, agreeing with the results in Hes5-overexpressing Tg mice (Bansod et al., 2017). Notably, many GFAP$^+$ cells appeared outside the VZ/SVZ and were scattered throughout the Tg cortex at P7 (Fig. 5B), whereas GFAP$^+$ cells were localized in the VZ/SVZ and superficial cortical layers of the WT brain. Similarly, many GFP$^+$ cells were scattered throughout the Tg cortex at P7 (Fig. 5B), although expression of d2EGFP was mostly restricted to the VZ/SVZ until P0 (Fig. 5A). Notably, those GFP$^+$ cells were negative for GFAP, and the expression of d2EGFP and GFAP was virtually non-overlapping in the Tg cortex (Fig. 5B). We observed that most GFP$^+$ cells were Pax6$^+$ but negative for neuronal markers such as NeuN (Fig. 5B). These results suggest that downregulation of Hes1 is necessary for terminal differentiation into mature (GFAP$^+$) astrocytes and that those GFP$^+$;Pax6$^+$ cells were immature astrocytes in which terminal differentiation/maturation was prevented. The ectopic distribution of immature astrocytes (Pax6$^+$) might have enhanced the production of GFAP$^+$ astrocytes throughout the cortex. In contrast, we did not detect any notable differences in the oligodendrocyte lineage development between the WT and Tg brains (Fig. S5).

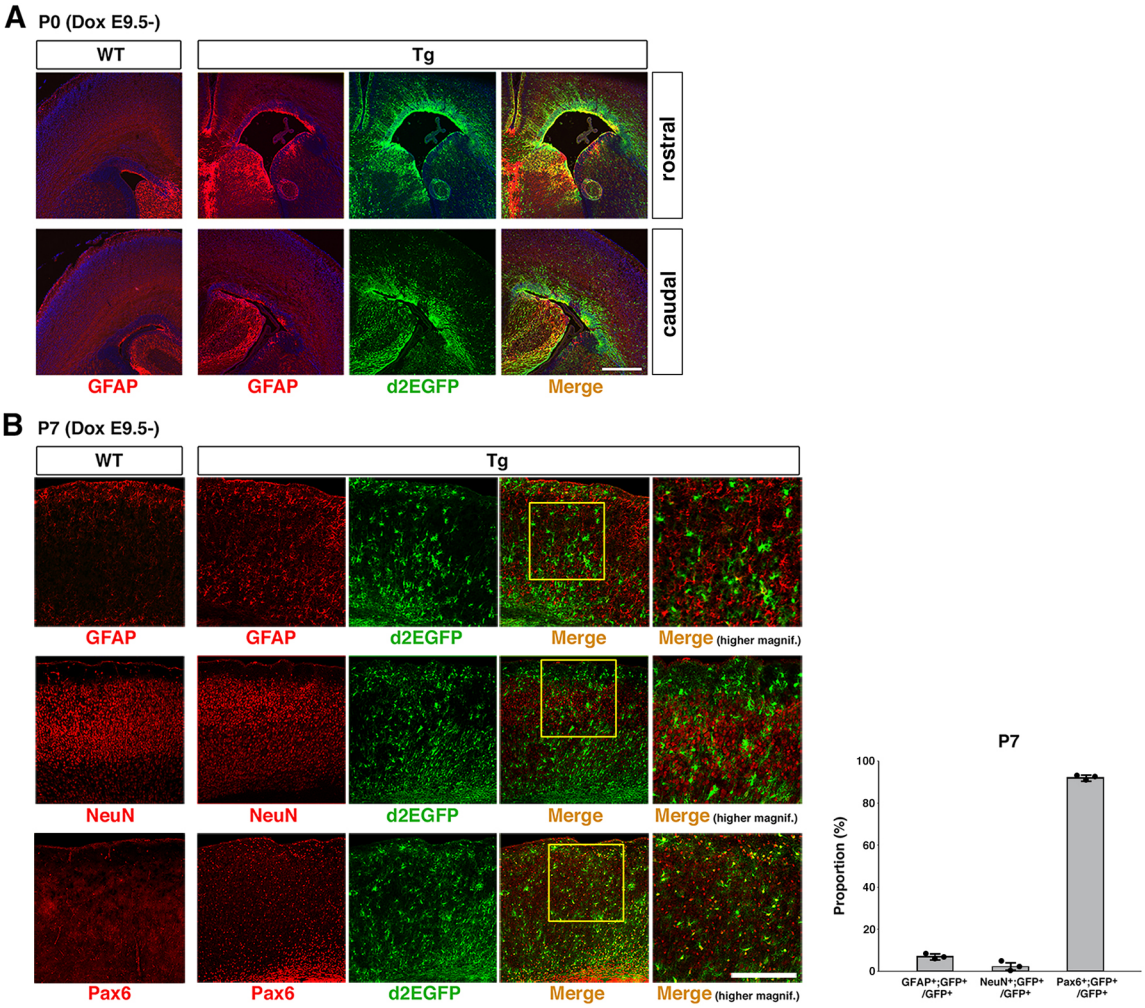

Fig. 5. Accelerated generation of GFAP-positive cells. (A) Double-labeling with anti-GFAP (red) and anti-GFP (green) antibodies on coronal sections of the telencephalon of WT and Tg mice at P0. Rostral and caudal regions of the telencephalon are shown in the upper and bottom rows, respectively. (B) Immunostaining with anti-GFAP, anti-NeuN or anti-Pax6 (red) antibody co-labeled with anti-GFP (green) antibody on coronal sections of dorsolateral cortex at P7. Higher magnification views of the boxed areas are shown in the rightmost panels. Graph shows the proportions of GFAP$^+$, NeuN$^+$ or Pax6$^+$ cells of GFP$^+$ cells in the Tg cortex at P7. Data are mean±s.e.m. (*n*=3). Scale bars: 500 µm in A; 200 µm in B.

Development (2021) 148, dev189191. doi:10.1242/dev.189191

Pax6$^+$ cells increased in contrast to a decrease in Tbr2$^+$ IPCs

It has been shown that the majority of superficial layer neurons are generated by repeated proliferation of Tbr2$^+$ IPCs in the SVZ (Tarabykin et al., 2001; Noctor et al., 2004; Arnold et al., 2008). Thus, we analyzed the number and proliferation rate of Tbr2$^+$ cells in the WT and Tg brains. The number of Tbr2$^+$ cells was not significantly different between WT and Tg mice until E13.5 (Fig. S6A). However, at later stages (E15.5 and E17.5), the number of Tbr2$^+$ IPCs in neocortical regions of the Tg brain was significantly less than that in the WT brain (Fig. 6A; Fig. S6A). pH3 staining also demonstrated that the number of dividing cells in both the VZ and SVZ of the Tg brain was significantly lower than that in the WT brain at E15.5 as shown in Fig. 3B, in agreement with the above observation that the number of Tbr2$^+$ IPCs was markedly diminished in the SVZ (Fig. 6A; Fig. S6A), in addition to the observation that the proliferation rate of Pax6$^+$ NSCs was suppressed in the VZ (Fig. S2A,C). However, double labeling using antibodies against Tbr2 and BrdU (administered 30 min before sacrifice) revealed that the proliferation rate of Tbr2$^+$ cells was not suppressed in the Tg brain and was comparable to that in the WT brain at E13.5 and E15.5 (Fig. S2B,D). These results suggest that the production of Tbr2$^+$ IPCs from NSCs was inhibited by Hes1 overexpression, potentially leading to the decelerated generation of later-born neurons.

Meanwhile, we noticed that Pax6$^+$ cells were remarkably increased in place of Tbr2$^+$ cells outside the VZ in the Tg brain at E17.5 (Fig. 6A). Double labeling for pH3 and Pax6 revealed significantly more pH3$^+$;Pax6$^+$ cells outside the VZ in the Tg brain at E15.5 and E17.5 (Fig. 6B, arrows), whereas in the WT brain, most pH3$^+$;Pax6$^+$ cells were located at the apical (ventricular) surface in the VZ where aRGCs are dividing in the M phase. We thus proceeded to characterize these pH3$^+$;Pax6$^+$ cells outside the VZ in more detail.

Basal radial glia-like cells were increased by Hes1 overexpression

It has been reported that bRGCs only retain basal radial processes, lack apical processes and are located in the SVZ (Wang et al., 2011). bRGCs manifest similar characteristics to those of aRGCs; they are positive for Hes1, Pax6 and Sox2, but negative for Tbr2. Thus, we examined whether the pH3$^+$;Pax6$^+$ cells outside the VZ in the Tg brain were bRGCs. We performed immunostaining with antibodies against phosphorylated vimentin (pVim), a specific marker of RGCs in the M phase (Kamei et al., 1998). Although pVim only labels a subset of RGCs that are dividing in the M phase, it is considered a useful marker to demonstrate increments in delaminated RGCs such as bRGCs (Pilz et al., 2013). Whereas pVim$^+$ cells were mostly restricted to the apical (ventricular) surface in the VZ where aRGCs are dividing, and only a few cells were aberrantly detected outside the VZ in the WT brain, pVim$^+$ cells markedly increased in number outside the VZ in the Tg brain at E17.5 (Fig. 6C,D). We confirmed that these aberrant pVim$^+$ cells were also positive for Pax6 (Fig. 6C) and pH3 (Fig. 6D), similar to dividing aRGCs.

We then attempted immunostaining with the RGC marker GLAST (Slc1a3), which labels radial fibers of RGCs. However, it was difficult to determine whether these pH3$^+$ cells in the SVZ were bRGCs that indeed lacked apical processes due to the exuberant radial fibers, although many pH3$^+$ cells in the SVZ were co-labeled with GLAST (Fig. S6B). Therefore, we introduced mCherry expression vectors (*pEF-mCherry*) into the VZ cells by *in utero* electroporation at E15.5 and analyzed the morphology of transfected cells at E17.5. Although the majority of transfected cells differentiated into neurons or remained as aRGCs in the VZ, a subset of mCherry$^+$ cells adopted a bRGC-like morphology; they were positive for Pax6 and located outside the VZ, retaining only basal radial processes but lacking apical processes (Fig. 6E; Fig. S6C, D; Movie 1). This suggested that a fraction of transfected cells transformed from aRGCs to bRGCs in the two days.

We further revealed that a majority of Pax6$^+$ cells outside the VZ in the Tg brain were positive for Neurog2 at E17.5, suggesting that they retained neurogenic potentials (Fig. 6F). These results collectively demonstrated that the number of bRGC-like cells increased at later embryonic stages following Hes1 overexpression, instead of the suppressed production of Tbr2$^+$ IPCs, in agreement with the localization patterns of Neurog2$^+$ cells (Fig. 2E,F) and Ccnd1$^+$ cells (Fig. 3F) in the SVZ. These findings suggested that, although switching from deep to superficial layer neurogenesis and onset of gliogenesis shifted earlier in neocortical regions of Tg brain, generation of superficial layer neurons was prolonged by neurogenesis from those bRGC-like cells in the SVZ, as illustrated by the schematic in Fig. 6G.

The adult NSC pool was expanded in Hes1-overexpressing Tg brain and adult neurogenesis was enhanced by attenuation of Hes1 expression

Next, we addressed whether NSCs were retained more abundantly and whether neurogenesis was enhanced in the postnatal and adult brains of Hes1-overexpressing Tg mice. Higher numbers of Hes1$^+$/d2EGFP$^+$ and Pax6$^+$ cells were observed in the SVZ of the rostral lateral ventricle, from which adult neurogenesis continues to supply newly born neurons to the olfactory bulbs, in postnatal (P14) and young adult (4 weeks after birth) Tg brains compared with the WT brains (Fig. 7A). We also observed that the expression of both d2EGFP and Hes1 was considerably diminished within 3 days after withdrawal of Dox in the Tg brain (4 weeks and 3 days) (Fig. 7A). Next, we estimated proliferation activity in the WT and Tg brains at 6 weeks after birth. When mice were administered with Dox from E11.5 to P35 (5 weeks) and sacrificed at P43 after 1-day administration of BrdU in drinking water from P42 (6 weeks), markedly more BrdU$^+$ cells were observed in the SVZ of the lateral ventricle in the Tg brains compared with the WT brains (Fig. 7B). We then performed immunostaining with antibodies against doublecortin (Dcx), a marker of newly born neurons. When mice were treated with Dox from E7.5 to P28 (4 weeks) and sacrificed at P31 after 3-day administration of BrdU in drinking water from P28, the number of Dcx$^+$ cells was markedly higher in the SVZ of the lateral ventricle in the Tg brains compared with the WT brains (Fig. 7C). Most of the Dcx$^+$ cells were BrdU$^+$, indicating that these cells incorporated BrdU and differentiated into neurons during the 3 days before sacrifice. These newly born neurons were broadly distributed along the extended ventricular surface. These results collectively implied the presence of an expanded NSC pool in the adult Tg brain, which retained the competence to continue adult neurogenesis and was enhanced by the attenuation of Hes1 expression (Fig. 7A,B).

Hes1 overexpression increased slowly-dividing cells that remained as postnatal NSCs

Furutachi et al. have reported the existence of a subpopulation of NSCs (that would be the origin of postnatal and adult NSCs) in the embryonic mouse brain from early developmental stages (Furutachi et al., 2015). Those NSCs were slowly-dividing and thus retained fluorescent marker proteins (GFP) without dilution until later stages. We therefore investigated whether the suppressed

Development (2021) 148, dev189191. doi:10.1242/dev.189191

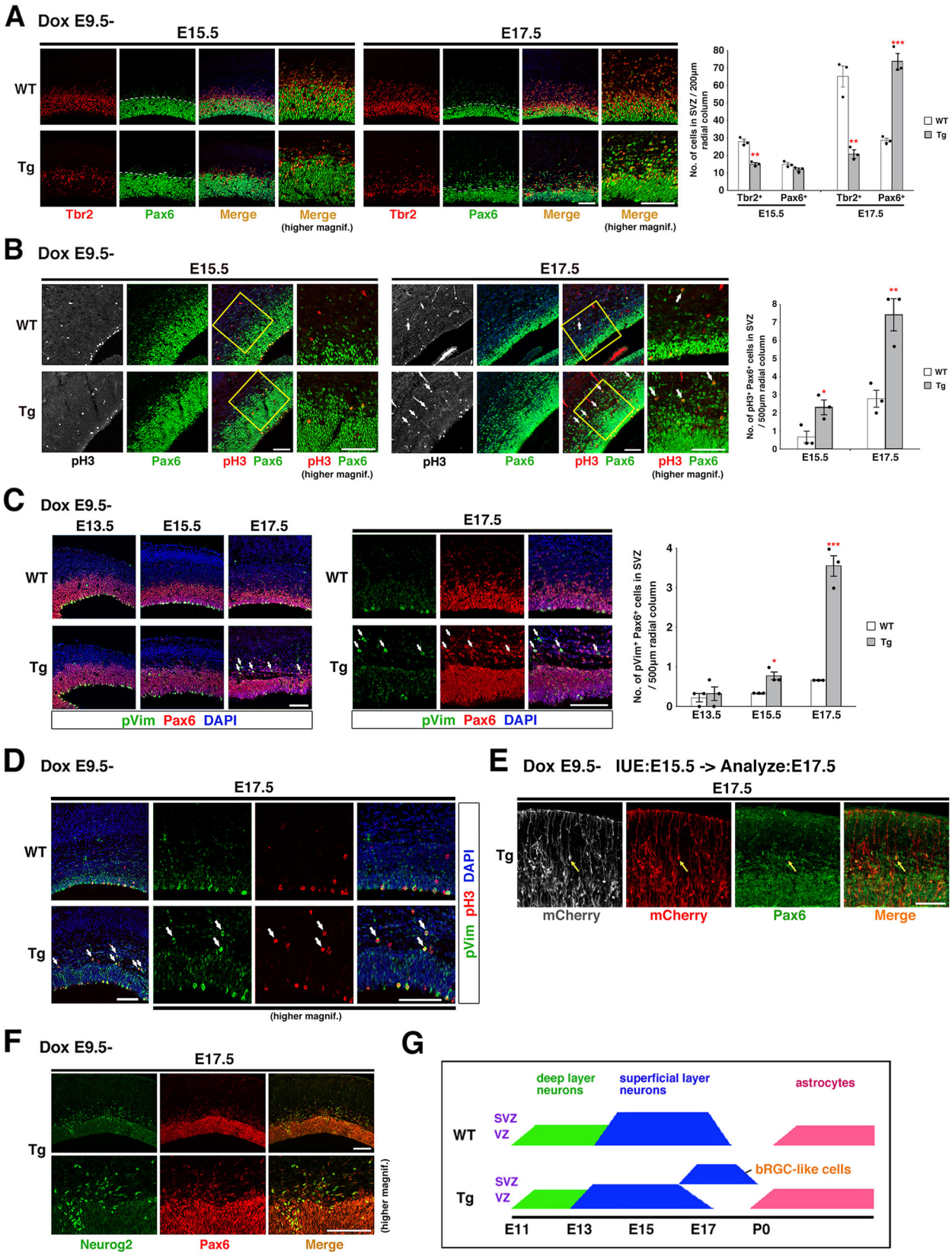

Fig. 6. See next page for legend.

proliferation rate caused by Hes1 overexpression led to the expansion of postnatal and adult NSCs. First, we administered EdU at E11.5 and estimated the retention of EdU in postnatal and adult SVZ cells. Many EdU label-retaining cells were observed in the dorsal and dorsolateral SVZ of the anterior lateral ventricle in the Hes1-overexpressing Tg brain at P0 (Fig. 7D, arrows), whereas only

Development (2021) 148, dev189191. doi:10.1242/dev.189191

Fig. 6. Increase in Pax6$^+$ bRGC-like cells instead of decrease in Tbr2$^+$ IPCs. (A) Double-labeling with anti-Tbr2 (red) and anti-Pax6 (green) antibodies on coronal sections of the neocortical regions of WT and Tg mice at E15.5 and E17.5. Borders of the VZ and SVZ were estimated based on the continuity of Pax6$^+$ cells and are shown by white dashed lines in green channels. Higher magnification views of merged images are shown in the rightmost panels. Quantification of the number of cells expressing each marker in the SVZ within a radial column of 200 µm width is shown on the right. (B) Double-labeling with anti-pH3 (red) and anti-Pax6 (green) antibodies on coronal sections of the dorsolateral telencephalon at E15.5 and E17.5. pH3 signals are shown in white on the left panels (grayscale). Higher magnification views of the boxed areas are shown in the rightmost panels. Arrows indicate cells double-positive for pH3 and Pax6 (pH3$^+$;Pax6$^+$) in the SVZ. Quantification of the number of pH3$^+$;Pax6$^+$ cells in the SVZ within a radial column of 500 µm width is shown on the right. (C) Double-labeling with anti-pVim (green) and anti-Pax6 (red) antibodies on coronal sections of neocortical regions at E13.5, E15.5 and E17.5. Arrows indicate pVim$^+$;Pax6$^+$ cells in the SVZ. Higher magnification views of E17.5 are shown in the panels on the right. Quantification of the number of pVim$^+$;Pax6$^+$ cells in the SVZ within a radial column of 500 µm width is shown on the right. (D) Double-labeling with anti-pVim (green) and anti-pH3 (red) antibodies on coronal sections of neocortical regions at E17.5. Arrows indicate pVim$^+$;pH3$^+$ cells in the SVZ. Higher magnification views are shown in the right panels. (E) *pEF-mCherry* expression vectors were transfected into the VZ cells of Tg embryos by *in utero* electroporation (IUE) at E15.5. The morphology of transfected cells was analyzed by immunohistochemistry with anti-mCherry (red) and anti-Pax6 (green) antibodies on coronal sections of neocortical regions at E17.5. The arrow indicates a mCherry$^+$;Pax6$^+$ cell with bRGC-like morphology that retains only basal radial processes but lacks apical processes and is located in the SVZ. (F) Double-labeling with anti-Neurog2 (green) and anti-Pax6 (red) antibodies on coronal sections of neocortical regions of Tg brain at E17.5. Higher magnification views are shown in the bottom panels. (G) Schematic demonstrating the different timing of neurogenesis and gliogenesis in WT and Tg cortices and prolonged neurogenesis from bRGC-like cells in the SVZ of Tg cortex. DAPI (blue) represents nuclear staining. Data are mean±s.e.m. (n=3). *P<0.05, **P<0.01, ***P<0.001 (unpaired two-tailed Student's t-test). Scale bars: 100 µm.

a few EdU label-retaining cells were observed in the SVZ of the WT brain. EdU label-retaining cells in the SVZ of the Tg brain were mostly Pax6$^+$, suggesting that these slowly-dividing cells remained as NSCs. Pax6$^+$ clusters sometimes exhibited rosette-like structures in the Tg brain, as shown in Fig. 7D, probably owing to the heterogeneous organization within the VZ/SVZ, although this phenotype was not typical nor reproducible. These results suggested that NSCs that strongly expressed Hes1 existed as slowly-dividing cells in the embryonic brain and remained as NSCs in postnatal and adult brains. Therefore, we next evaluated Hes1 expression levels in EdU label-retaining cells in the WT brain using anti-Hes1 antibody to verify whether NSCs that expressed higher levels of endogenous Hes1 remained as slowly-dividing NSCs in postnatal and adult brains. However, we did not detect significantly higher levels of Hes1 expression in EdU label-retaining cells in the SVZ of embryonic and postnatal brains (Fig. S7). These results suggested that, although Hes1 can expand the NSC reservoir in the adult brain, it is not involved in formation of endogenous adult NSCs.

DISCUSSION

Overexpression of Hes1 maintains NSCs but suppresses cell proliferation

In the embryonic brains of Hes1-overexpressing Tg mice, neuronal differentiation was suppressed and NSCs were maintained in the enlarged VZ. As NSCs continued symmetric proliferative divisions (Fig. 3E), the VZ extended tangentially, and the ventricular surface and ventricles were expanded (Fig. 2A,B). Furthermore, we observed that the number of Pax6$^+$ NSCs was increased in the Tg brain (Fig. 2B), although the proliferation rate of NSCs was reduced, as shown in Fig. 3. This result indicated that the increase of Pax6$^+$ NSCs owing to the elongation of the period of symmetric proliferative divisions prevailed over their low proliferation rate.

Regardless of the expansion of NSCs in embryonic brains, Hes1-overexpressing Tg mice exhibited smaller brains and bodies (Fig. S1). This is partly because inhibition of neuronal differentiation impaired brain maturation. Actually, both the cortical wall and ventral part of the telencephalon were thinner, and some brain structures such as the hippocampus and corpus callosum appeared to be hypoplastic in Tg mice compared with WT mice. In addition, suppression of cell proliferation by Hes1 overexpression may have contributed. It has been reported that the appropriate levels of Hes1 promote cell proliferation (Murata et al., 2005) but, on the other hand, Hes1 overexpression inhibits cell proliferation (Baek et al., 2006; Shi et al., 2015). Several cell cycle-related genes were found to be repressed by Hes1 (Georgia et al., 2006; Monahan et al., 2009), and we have previously demonstrated using cDNA microarrays that *Ccnd1* expression was downregulated by Hes1 overexpression (Shimojo et al., 2008). Here, we confirmed that Ccnd1 expression was indeed suppressed in the VZ of Hes1-overexpressing Tg brain compared with the WT brain. We hypothesized that abolishing exogenous Hes1 expression by withdrawal of Dox would induces active neurogenesis and increases neuronal number and brain size, as NSC numbers were increased at ∼E15.5 and thereafter. We attempted the withdrawal of Dox at various developmental stages but failed to observe larger brains in Tg mice. Thus, it would be a forthcoming challenge to test whether it is possible to achieve brain expansion by rescuing cell cycle-related genes such as *Ccnd1* to release the blockade of cell cycle progression.

Hes1 overexpression promotes the generation of Pax6$^+$ bRGC-like cells at the expense of Tbr2$^+$ IPCs

In certain mammalian species such as dogs, sheep and primates, the brain surface is convoluted (gyrencephalic), in contrast to the smooth brain surface of lissencephalic mammals such as mice, and it has been thought that mammals have developed gyrencephalic brains during mammalian evolution. It has been revealed that the development of OSVZ and bRGCs led to the expansion of the stem cell pool, increased production of superficial layer neurons, and promoted enlargement of the brain surface.

In the Hes1-overexpressing Tg brains at late embryonic stages, many pH3$^+$;Pax6$^+$ cells were scattered in the SVZ, whereas Tbr2$^+$ IPCs were decreased in number. We attempted to characterize these Pax6$^+$ cells outside the VZ to elucidate whether they have morphology and properties corresponding to bRGCs, but it was highly challenging to identify what proportion of these cells were bRGCs owing to the lack of specific markers for bRGCs. However, based on complementary experiments, a subset of these cells appeared to exhibit bRGC-like morphology and properties, and pVim staining revealed a marked increment in the number of mitotic RGCs in the SVZ of neocortical regions in the Tg brain. Although the mechanisms underlying the enhanced production of bRGC-like cells by Hes1 overexpression remain unclear, it is possible that high levels of Hes1 forcibly arrested neuronal differentiation of prospective neuronal daughters after asymmetric divisions of aRGCs, which normally produce a stem cell daughter and neuronal daughter, and retained them as bRGC-like NSCs in the SVZ. This prevention of the production of neuronal daughters may account for the reduction in Tbr2$^+$ IPCs in the SVZ. Growing evidence revealed the involvement of various genes and signaling pathways in the generation and expansion of bRGCs (Penisson et al., 2019).

Development (2021) 148, dev189191. doi:10.1242/dev.189191

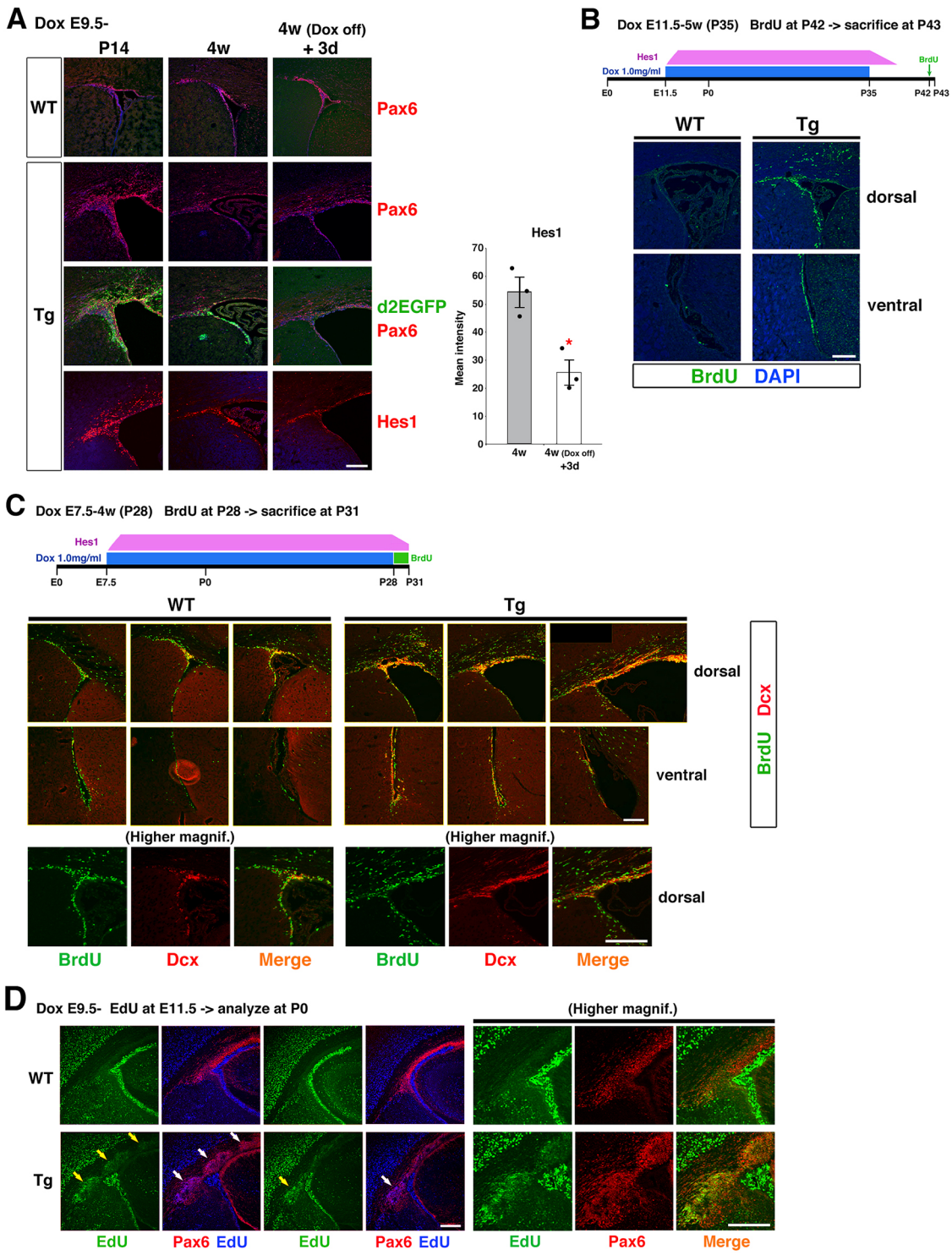

Fig. 7. See next page for legend.

However, there have been few studies that demonstrated the direct contribution of Notch signaling to enhanced generation of bRGCs, although Shitamukai et al. reported the implication of Notch signaling in the retainment of basal processes of NSCs and the maintenance of newly born bRGC-like cells (Shitamukai et al., 2011). Our findings provided further supportive evidence implicating the contribution of Notch signaling to the expansion of bRGCs during mammalian brain evolution.

Expansion of both basal progenitors (bRGCs and IPCs) appears to be necessary to achieve neocortical expansion as seen in gyrencephalic mammals. Nevertheless, in the Hes1-overexpressing Tg brain, only bRGC-like cells increased at the expense of IPCs, leading to failure of neocortical expansion. To achieve a bigger brain with a larger neocortical surface, alternative strategies for promoting the production and proliferation of IPCs while maintaining NSCs (aRGCs and bRGCs) would be required.

Development (2021) 148, dev189191. doi:10.1242/dev.189191

Fig. 7. Enhanced neurogenesis in the adult SVZ. (A) Immunostaining with anti-Pax6 (red), anti-GFP (green) and anti-Hes1 (red) antibodies on coronal sections of the postnatal and adult brains, including the regions surrounding the SVZ of the lateral ventricles, at P14, P28 (4 weeks) and P28 (4 weeks)+3 days (Dox administration was stopped at P28, and mice were sacrificed 3 days later). Graph shows the Hes1 expression levels in the SVZ of Tg brains at 4 weeks after birth and 3 days after withdrawal of Dox (4 weeks and 3 days). (B) Analysis of cell proliferation in adult brains of WT and Tg mice. Dox administration in drinking water was commenced at E11.5 and terminated at P35 (5 weeks). Mice were subjected to intraperitoneal injection of BrdU at P42 (6 weeks) and sacrificed at P43. Proliferative cells that incorporated BrdU were detected by immunohistochemistry with anti-BrdU (green) antibody. Coronal sections of dorsal and ventral regions surrounding the lateral ventricles are shown in upper and bottom rows, respectively. (C) Analysis of adult neurogenesis in WT and Tg brains. Dox administration in drinking water was commenced at E7.5 and terminated at P28 (4 weeks). Mice were sacrificed at P31 after 3-day administration of BrdU in drinking water from P28. Newly born neurons that incorporated BrdU were detected by double-labeling with anti-BrdU (green) and anti-Dcx (red) antibodies on coronal sections of dorsal (upper) and ventral (lower) regions surrounding the lateral ventricles. Panels are arranged in order from anterior (left) to posterior (right) brain regions along the anterior-posterior axis. Higher magnification views of dorsal regions are shown in the bottom panels. The right upper panel was created by assembling two images. The region enclosing the dorsal SVZ was cropped and the blank area at the upper left corner was painted black. (D) Estimation of EdU label-retaining cells in the SVZ; single-labeling of EdU (green) (left columns) and double-labeling of Pax6 (red) and EdU (blue) (right columns) on coronal sections at P0. EdU was injected intraperitoneally into pregnant mice at E11.5 and detected by Click reaction at P0. Note that the choroid plexus epithelial cells that incorporated EdU at E11.5 remain as EdU^+ cells in the lateral ventricle, and that EdU^+ cells were rarely observed in the SVZ of WT brain, whereas many EdU^+ cells were observed in the dorsal and dorsolateral SVZ of Tg brain (arrows). Higher magnification views are shown in the right panels. DAPI (blue) represents nuclear staining. Data are mean±s.e.m. (n=3). *P<0.05 (unpaired two-tailed Student's t-test). Scale bars: 200 µm.

Hes1 overexpression leads to expansion of the NSC reservoir enabling enhanced neurogenesis in the adult brain

It is well established that neurogenesis continues in specific regions of the adult brain: the SVZ of the rostral lateral ventricle and the dentate gyrus of the hippocampus. NSCs in these neurogenic regions gradually decline in number, and neurogenesis is attenuated with aging. We observed substantially more $Pax6^+$ cells in the SVZ of postnatal and adult brains of Hes1-overexpressing Tg mice, especially in the dorsal telencephalon. Moreover, we observed an enhanced generation of Dcx^+ cells in the dorsal and lateral part of the enlarged SVZ in the adult Tg brain, when Dox was withdrawn several days before sacrifice, thereby attenuating Hes1 expression and releasing subsequent inhibition of neuronal differentiation. These results suggest that elevation of Hes1 expression levels in NSCs results in expansion of the NSC reservoir with neurogenic potential. Conventional therapeutic strategies are aimed at compensating for the declined neurogenesis in aged brains or brains of neurodegenerative disorders, such as Alzheimer's disease, by maintaining adult NSCs and enhancing adult neurogenesis by activating pre-existing quiescent NSCs. In contrast, our study sheds light on the unexploited aspect of neuroregenerative therapy by aiming to expand the NSC reservoir with the potential to generate neurons to replenish impaired brain regions, leading to improved regenerative capacity against brain damage or neurodegenerative disorders.

Another candidate resource of newly born neurons is the GFP^+; $Pax6^+$ cell population observed throughout the neocortex of postnatal Tg brains (Fig. 5B). It is possible that these cells are immature glial cells in which further differentiation/maturation is suppressed by Hes1 overexpression. In other words, this suggests that downregulation of Hes1 is necessary for terminal differentiation into mature ($GFAP^+$) astrocytes. These cells may retain stemness or have the potential to dedifferentiate and commence neurogenesis. Thus, investigating whether these cells produce new neurons when brain tissues are damaged by physical injury, ischemia or neurodegeneration will be of interest. Unfortunately, rtTA expression in the hippocampus was very weak, and we could not detect GFP expression in the hippocampus of the postnatal Tg brain. Therefore, it was difficult to analyze the effect of Hes1 overexpression on NSCs in the hippocampus, including the dentate gyrus.

We observed that many NSCs with low proliferation rate due to Hes1 overexpression were maintained as EdU label-retaining $Pax6^+$ cells in the dorsal and dorsolateral SVZ of the postnatal Tg brain. This result suggests that slowly-dividing NSCs more likely remain as NSCs in postnatal and adult brains, in agreement with a previous report (Furutachi et al., 2015). Therefore, we expected expression levels of endogenous Hes1 to be higher in slowly-dividing NSCs (prospective adult NSCs) during normal brain development. However, we observed that Hes1 expression levels were not significantly higher in EdU label-retaining cells in the postnatal WT brain. This result indicates that high levels of Hes1 expression are sufficient to maintain slowly-dividing NSCs as postnatal NSCs but are not essential for the retention of slowly-dividing NSCs during normal brain development. This suggests that the proliferation rate of NSCs is regulated by other factors with activities similar to those of Hes1, such as other Hes family, Hes-related factors, Id protein family, or other cell cycle regulatory proteins. In this context, it was reported that inactivation of Hes1, Hes3, Hes5 and Hey1 depleted virtually all NSCs in the adult brain (Sueda et al., 2019). Uncovering the mechanisms underlying the maintenance of adult NSCs and establishing effective measures to expand them will enable brain modifications to promote higher regenerative capacity.

MATERIALS AND METHODS

Generation of Hes1-overexpressing mice

For *pNestin-rtTA* transgene, an 8-kb *Sma*I fragment containing the ZGF cassette, which has a 5.8-kb fragment of the *Nestin* promoter region, polyadenylation sequence of SV40, and 1.8-kb fragment of the second intron of *Nestin* gene (Mignone et al., 2004), was subcloned into the *Sal*I site of *pBluescript SK-* vector using *Not*I linkers (Takara). A 0.8-kb *rtTA-Advanced* fragment was excised from *pTet-On Advanced* vector (Clontech Laboratories) by *Eco*RI-*BamH*I digestion and subcloned into the *Sal*I site downstream of the *Nestin* promoter using *Sal*I linkers (Takara). For microinjection, the 8.8-kb *Not*I fragment containing the transgene was separated by agarose gel electrophoresis, purified using QIAEXII Gel Extraction Kit (Qiagen), and eluted with TE. For *TRE-Hes1/d2EGFP* transgene, a 0.9-kb fragment of mouse *Hes1* cDNA with *Cla*I linkers and a 0.9-kb *BamH*I-*Not*I fragment of *d2EGFP* from the *pd2EGFP-1* vector (Clontech Laboratories) with *Eco*RI linkers were inserted into MCS-I and MCS-II of the *pTRE-Tight-BI* vector (Clontech Laboratories), respectively (Fig. 1A). For microinjection, a 2.9-kb fragment containing the bilateral expression cassette from polyA for MCS-I to polyA for MCS-II was excised using *Nsp*I-*BspH*I, separated by agarose gel electrophoresis, purified using QIAEXII Gel Extraction Kit, and eluted with TE.

Transgenic mice were generated by pronuclear microinjection using fertilized eggs from ICR mice. Transgenic founders and progeny were identified by PCR analysis of tail DNA using primers that amplified the full-length of rtTA, Hes1, or d2EGFP. Both lines were crossed and doxycycline hyclate (Sigma-Aldrich; 1.0 mg/ml) in drinking water with 5% sucrose was administered to pregnant mice. Double transgenic mice were identified by PCR analysis and judged by GFP fluorescence in the brain and eyes. Images of whole bodies and brains with GFP fluorescence were obtained with a MZ16FA fluorescence stereo microscope equipped with a DFC300 FX

Development (2021) 148, dev189191. doi:10.1242/dev.189191

digital camera (Leica). Animal experiments were carried out according to the guidelines for animal experiments at Kyoto University.

Immunohistochemistry

For immunohistochemical analysis, brains were excised, fixed in 4% paraformaldehyde (PFA), cryoprotected, embedded in OCT compound, and cryosectioned at 16 µm. Fixed cryosections were washed with phosphate-buffered saline (PBS), preincubated in PBS containing 5% normal goat serum and 0.1% Triton X-100, then incubated in 1% normal goat serum and 0.1% Triton X-100 with primary antibodies overnight at 4°C followed by secondary antibodies for 1–3 h at room temperature. Primary antibodies used in this study are listed in Table S1. Primary antibodies were detected with Alexa Fluor-conjugated secondary antibodies (1:200; Molecular Probes), and cell nuclei were visualized with 4′,6-diamidino-2-phenylindole (DAPI; Sigma-Aldrich). For Hes1 staining, antigen retrieval was performed in 0.1% Tween 20/0.01 M citrate buffer (pH 6.0) using an autoclave for 15 min at 105°C, and sections were incubated with primary antibodies in Can Get Signal Solution B (Toyobo) overnight at 4°C followed by secondary antibodies (HRP-conjugated donkey anti-rabbit IgG, 1:500; GE Healthcare) for 90 min at room temperature. Color development was enhanced by the TSA amplification system (PerkinElmer) according to the manufacturer's instruction. Fluorescent sections were imaged using a Zeiss LSM510 confocal microscope or a Keyence BZ-X700 fluorescence microscope.

Quantitative real-time RT-PCR

Total RNA was prepared from the dorsolateral telencephalon (neocortical regions) of mouse brains as previously described (Ohtsuka et al., 2011). Reverse transcription was performed using total RNA as previously described (Tan et al., 2012). *Gapdh* was used as an internal control. PCR primers are listed in Table S2.

In situ hybridization

In situ hybridization was performed as previously described (Ohtsuka et al., 2011). Digoxigenin-labeled antisense RNA probes were synthesized *in vitro* using the full-length cDNAs of *Hes1* (NM_008235.2) and *Neurog2* (NM_009718.2) as templates, and hybridized to brain cryosections. Labeled preparations were imaged using a Zeiss Axiophot microscope equipped with an AxioCam color CCD camera.

BrdU labeling and birth date analysis

To analyze the cell proliferation rate, 5-bromo-2′-deoxyuridine (BrdU; Sigma-Aldrich) (50 µg BrdU/g of body weight) was injected intraperitoneally into pregnant mice 30 min before sacrifice, and embryonic brains were fixed with 4% PFA. For the birth date analysis, we conducted a double pulse labeling of DNA synthesis using BrdU and 5-iodo-2′-deoxyuridine (IdU; Sigma-Aldrich). BrdU (50 µg BrdU/g of body weight) or IdU (50 µg IdU/g of body weight) was injected intraperitoneally into pregnant mice at different embryonic stages, and brains were fixed by transcardial perfusion with 4% PFA at postnatal day 14 (P14). The fixed cryosections were incubated in 2 N HCl solution for 30 min at 37°C, followed by neutralization in 0.1 M sodium tetraborate buffer. Sections were incubated with mouse anti-BrdU antibody (1:100; Becton Dickinson) and rat anti-BrdU antibody (1:500; Serotec) overnight at 4°C, and then with Alexa594-conjugated goat anti-mouse IgG and Alexa488-conjugated goat anti-rat IgG (1:200; Molecular Probes). As mouse anti-BrdU antibody reacts with both BrdU and IdU whereas rat anti-BrdU antibody reacts only with BrdU, cells that incorporated IdU were stained in red whereas cells that incorporated BrdU were depicted in yellow (red+green).

Analysis of cell cycle length of NSCs

Estimation of the cell cycle length was performed as previously described (Watanabe et al., 2015). We conducted a dual pulse labeling of DNA synthesis using BrdU and EdU (5-ethynyl-2′-deoxyuridine) (Molecular Probes), referring to the previous methods (Martynoga et al., 2005; Mairet-Coello et al., 2012). BrdU (50 µg BrdU/g of body weight) and EdU (12.5 µg EdU/g of body weight) were injected intraperitoneally into pregnant mice 2 h and 30 min before sacrifice, respectively, and the ratios of $Pax6^+$ cells that incorporated either or both BrdU and EdU were analyzed to estimate the cell cycle length.

Plasmid construction and *in utero* electroporation

For the *pEF-mCherry* vector, the coding sequence of *mCherry* was cloned into the *pEF* (human elongation factor 1α promoter)-*MM* expression vector, which was modified from the *pEF-BOS* vector (Mizushima and Nagata, 1990). To label the basal radial glia-like cells, *in utero* electroporation was performed with E15.5 pregnant mice using methods described previously (Ohtsuka et al., 2011). Embryos were harvested 2 days after electroporation at E17.5. Brains were excised, fixed in 4% PFA, cryoprotected, embedded in OCT, and cryosectioned at 16-70 µm.

Estimation of symmetric vs asymmetric division of NSCs

To estimate the division mode (symmetric vs asymmetric division) of NSCs, we first performed *in utero* electroporation using the *pEF-mCherry* vector to only label the VZ cells (apical NSCs) at E13.5. EdU (12.5 µg EdU/g of body weight) was injected intraperitoneally into pregnant mice 6 h after *in utero* electroporation, and mice were sacrificed 18 h after EdU injection at E14.5. The numbers of $Pax6^+$;EdU^+/EdU^+ cells and $Tbr2^+$;EdU^+/EdU^+ cells were counted within a radial column of 200 µm width on the coronal sections of neocortical regions.

Estimation of EdU label-retaining cells

EdU (12.5 µg EdU/g of body weight) was injected intraperitoneally into pregnant mice at E11.5, and the detection of EdU-labeled cells was performed based on a fluorogenic click reaction (Salic and Mitchison, 2008) at P0.

Creation of 3D movie file

Fixed and cryoprotected brains were cryosectioned at 70 µm. Fixed cryosections were incubated with anti-mCherry antibody 2-3 overnight at 4°C followed by secondary antibody for 2-3 h at room temperature. Fluorescent images were taken using a Zeiss LSM510 confocal microscope, combined to create *z*-stack images including full-thickness of brain sections, and converted to 3D movies using ImageJ/Fiji (NIH, USA).

Measurement

Cell numbers within a radial column of 200 µm width (Figs 2B, 3A-C,E,F, 4A,B and 6A, Figs S2C,D, and S6A), 500 µm width (Fig. 6B,C), or 1 mm width (Fig. 4G) on the coronal sections of neocortical regions were counted. In Fig. 4H, cell numbers in a 450 µm×450 µm square in the cortex and those within a radial column of 450 µm width in the SVZ of cortical area were counted. In Fig. 5B, cell numbers in a 500 µm×500 µm square in the cortex were counted. The measurement of the length of ventricular and cortical surface (from the dorsal ridge to the dorsolateral border) was performed by using ImageJ/Fiji. Hes1 expression level in the postnatal SVZ was analyzed by measuring the signal intensity of Hes1 immunostaining in a 500 µm×100 µm strip in the SVZ along the lateral ventricular surface by using ImageJ/Fiji.

Statistical analysis

Each experiment was performed with at least three independent samples. Results are shown as mean±s.e.m. Statistical differences were examined with unpaired two-tailed Student's *t*-test.

Acknowledgements

We thank Hitoshi Miyachi and Satsuki Kitano for their help in the generation of *pNestin-rtTA* transgenic mice and *TRE-Hes1/d2EGFP* transgenic mice.

Competing interests

The authors declare no competing or financial interests.

Author contributions

Conceptualization: T.O.; Methodology: T.O.; Formal analysis: T.O.; Investigation: T.O.; Writing - original draft: T.O.; Supervision: R.K.; Project administration: T.O.; Funding acquisition: T.O., R.K.

Funding
This work was supported by Core Research for Evolutional Science and Technology (JPMJCR12W2 to R.K.), Grant-in-Aid for Scientific Research on Innovative Areas from the Ministry of Education, Culture, Sports, Science and Technology (16H06480 to R.K.), and Grant-in-Aid for Scientific Research from the Japan Society for the Promotion of Science (15H02349 to R.K.; 23500390, 15K06773 and 18K06253 to T.O.).

Supplementary information
Supplementary information available online at
https://dev.biologists.org/lookup/doi/10.1242/dev.189191.supplemental

Peer review history
The peer review history is available online at
https://dev.biologists.org/lookup/doi/10.1242/dev.189191.reviewer-comments.pdf

References

Arnold, S. J., Huang, G.-J., Cheung, A. F. P., Era, T., Nishikawa, S.-I., Bikoff, E. K., Molnár, Z., Robertson, E. J. and Groszer, M. (2008). The T-box transcription factor Eomes/Tbr2 regulates neurogenesis in the cortical subventricular zone. *Genes Dev.* **22**, 2479-2484. doi:10.1101/gad.475408

Baek, J. H., Hatakeyama, J., Sakamoto, S., Ohtsuka, T. and Kageyama, R. (2006). Persistent and high levels of Hes1 expression regulate boundary formation in the developing central nervous system. *Development* **133**, 2467-2476. doi:10.1242/dev.02403

Bansod, S., Kageyama, R. and Ohtsuka, T. (2017). Hes5 regulates the transition timing of neurogenesis and gliogenesis in mammalian neocortical development. *Development* **144**, 3156-3167. doi:10.1242/dev.147256

Cau, E., Gradwohl, G., Casarosa, S., Kageyama, R. and Guillemot, F. (2000). Hes genes regulate sequential stages of neurogenesis in the olfactory epithelium. *Development* **127**, 2323-2332.

Furutachi, S., Miya, H., Watanabe, T., Kawai, H., Yamasaki, N., Harada, Y., Imayoshi, I., Nelson, M., Nakayama, K. I., Hirabayashi, Y. et al. (2015). Slowly dividing neural progenitors are an embryonic origin of adult neural stem cells. *Nat. Neurosci.* **18**, 657-665. doi:10.1038/nn.3989

Georgia, S., Soliz, R., Li, M., Zhang, P. and Bhushan, A. (2006). p57 and Hes1 coordinate cell cycle exit with self-renewal of pancreatic progenitors. *Dev. Biol.* **298**, 22-31. doi:10.1016/j.ydbio.2006.05.036

Hansen, D. V., Lui, J. H., Parker, P. R. L. and Kriegstein, A. R. (2010). Neurogenic radial glia in the outer subventricular zone of human neocortex. *Nature.* **464**, 554-561. doi:10.1038/nature08845

Hatakeyama, J., Bessho, Y., Katoh, K., Ookawara, S., Fujioka, M., Guillemot, F. and Kageyama, R. (2004). Hes genes regulate size, shape and histogenesis of the nervous system by control of the timing of neural stem cell differentiation. *Development* **131**, 5539-5550. doi:10.1242/dev.01436

Hevner, R. F. and Haydar, T. F. (2012). The (not necessarily) convoluted role of basal radial glia in cortical neurogenesis. *Cereb. Cortex* **22**, 465-468. doi:10.1093/cercor/bhr336

Hirata, H., Ohtsuka, T., Bessho, Y. and Kageyama, R. (2000). Generation of structurally and functionally distinct factors from the basic helix-loop-helix gene Hes3 by alternative first exons. *J. Biol. Chem.* **275**, 19083-19089. doi:10.1074/jbc.M001075200

Hirata, H., Tomita, K., Bessho, Y. and Kageyama, R. (2001). Hes1 and Hes3 regulate maintenance of the isthmic organizer and development of the mid/hindbrain. *EMBO J.* **20**, 4454-4466. doi:10.1093/emboj/20.16.4454

Imayoshi, I., Sakamoto, M., Ohtsuka, T., Takao, K., Miyakawa, T., Yamaguchi, M., Mori, K., Ikeda, T., Itohara, S. and Kageyama, R. (2008). Roles of continuous neurogenesis in the structural and functional integrity of the adult forebrain. *Nat. Neurosci.* **11**, 1153-1161. doi:10.1038/nn.2185

Ishibashi, M., Moriyoshi, K., Sasai, Y., Shiota, K., Nakanishi, S. and Kageyama, R. (1994). Persistent expression of helix-loop-helix factor HES-1 prevents mammalian neural differentiation in the central nervous system. *EMBO J.* **13**, 1799-1805. doi:10.1002/j.1460-2075.1994.tb06448.x

Ishibashi, M., Ang, S. L., Shiota, K., Nakanishi, S., Kageyama, R. and Guillemot, F. (1995). Targeted disruption of mammalian hairy and enhancer of split homolog-1 (HES-1) leads to up-regulation of neural helix-loop-helix factors, premature neurogenesis, and severe neural tube defects. *Genes Dev.* **9**, 3136-3148. doi:10.1101/gad.9.24.3136

Kageyama, R. and Ohtsuka, T. (1999). The notch-hes pathway in mammalian neural development. *Cell Res.* **9**, 179-188. doi:10.1038/sj.cr.7290016

Kamei, Y., Inagaki, N., Nishizawa, M., Tsutsumi, O., Taketani, Y. and Inagaki, M. (1998). Visualization of mitotic radial glial lineage cells in the developing rat brain by Cdc2 kinase-phosphorylated vimentin. *Glia* **23**, 191-199. doi:10.1002/(SICI)1098-1136(199807)23:3<191::AID-GLIA2>3.0.CO;2-8

LaMonica, B. E., Lui, J. H., Wang, X. and Kriegstein, A. R. (2012). OSVZ progenitors in the human cortex: an updated perspective on neurodevelopmental disease. *Curr. Opin. Neurobiol.* **22**, 747-753. doi:10.1016/j.conb.2012.03.006

Lui, J. H., Hansen, D. V. and Kriegstein, A. R. (2011). Development and evolution of the human neocortex. *Cell* **146**, 18-36. doi:10.1016/j.cell.2011.06.030

Mairet-Coello, G., Tury, A., Van Buskirk, E., Robinson, K., Genestine, M. and DiCicco-Bloom, E. (2012). $p57^{KIP2}$ regulates radial glia and intermediate precursor cell cycle dynamics and lower layer neurogenesis in developing cerebral cortex. *Development* **139**, 475-487. doi:10.1242/dev.067314

Martynoga, B., Morrison, H., Price, D. J. and Mason, J. O. (2005). Foxg1 is required for specification of ventral telencephalon and region-specific regulation of dorsal telencephalic precursor proliferation and apoptosis. *Dev. Biol.* **283**, 113-127. doi:10.1016/j.ydbio.2005.04.005

Mignone, J. L., Kukekov, V., Chiang, A.-S., Steindler, D. and Enikolopov, G. (2004). Neural stem and progenitor cells in nestin-GFP transgenic mice. *J. Comp. Neurol.* **469**, 311-324. doi:10.1002/cne.10964

Mizushima, S. and Nagata, S. (1990). pEF-BOS, a powerful mammalian expression vector. *Nucleic Acids Res.* **18**, 5322. doi:10.1093/nar/18.17.5322

Molnár, Z., Vasistha, N. A. and Garcia-Moreno, F. (2011). Hanging by the tail: progenitor populations proliferate. *Nat. Neurosci.* **14**, 538-540. doi:10.1038/nn.2817

Monahan, P., Rybak, S. and Raetzman, L. T. (2009). The notch target gene HES1 regulates cell cycle inhibitor expression in the developing pituitary. *Endocrinology* **150**, 4386-4394. doi:10.1210/en.2009-0206

Murata, K., Hattori, M., Hirai, N., Shinozuka, Y., Hirata, H., Kageyama, R., Sakai, T. and Minato, N. (2005). Hes1 directly controls cell proliferation through the transcriptional repression of p27Kip1. *Mol. Cell. Biol.* **25**, 4262-4271. doi:10.1128/MCB.25.10.4262-4271.2005

Noctor, S. C., Martínez-Cerdeño, V., Ivic, L. and Kriegstein, A. R. (2004). Cortical neurons arise in symmetric and asymmetric division zones and migrate through specific phases. *Nat. Neurosci.* **7**, 136-144. doi:10.1038/nn1172

Ohtsuka, T., Ishibashi, M., Gradwohl, G., Nakanishi, S., Guillemot, F. and Kageyama, R. (1999). Hes1 and Hes5 as notch effectors in mammalian neuronal differentiation. *EMBO J.* **18**, 2196-2207. doi:10.1093/emboj/18.8.2196

Ohtsuka, T., Sakamoto, M., Guillemot, F. and Kageyama, R. (2001). Roles of the basic helix-loop-helix genes Hes1 and Hes5 in expansion of neural stem cells of the developing brain. *J. Biol. Chem.* **276**, 30467-30474. doi:10.1074/jbc.M102420200

Ohtsuka, T., Shimojo, H., Matsunaga, M., Watanabe, N., Kometani, K., Minato, N. and Kageyama, R. (2011). Gene expression profiling of neural stem cells and identification of regulators of neural differentiation during cortical development. *Stem Cells* **29**, 1817-1828. doi:10.1002/stem.731

Penisson, M., Ladewig, J., Belvindrah, R. and Francis, F. (2019). Genes and mechanisms involved in the generation and amplification of basal radial glial cells. *Front. Cell. Neurosci.* **13**, 381. doi:10.3389/fncel.2019.00381

Pilz, G.-A., Shitamukai, A., Reillo, I., Pacary, E., Schwausch, J., Stahl, R., Ninkovic, J., Snippert, H. J., Clevers, H., Godinho, L. et al. (2013). Amplification of progenitors in the mammalian telencephalon includes a new radial glial cell type. *Nat. Commun.* **4**, 2125. doi:10.1038/ncomms3125

Reillo, I., de Juan Romero, C., García-Cabezas, M. Á. and Borrell, V. (2011). A role for intermediate radial glia in the tangential expansion of the mammalian cerebral cortex. *Cereb. Cortex* **21**, 1674-1694. doi:10.1093/cercor/bhq238

Sakamoto, M., Imayoshi, I., Ohtsuka, T., Yamaguchi, M., Mori, K. and Kageyama, R. (2011). Continuous neurogenesis in the adult forebrain is required for innate olfactory responses. *Proc. Natl. Acad. Sci. USA* **108**, 8479-8484. doi:10.1073/pnas.1018782108

Salic, A. and Mitchison, T. J. (2008). A chemical method for fast and sensitive detection of DNA synthesis in vivo. *Proc. Natl. Acad. Sci. USA* **105**, 2415-2420. doi:10.1073/pnas.0712168105

Shi, X., Yan, C., Liu, B., Yang, C., Nie, X., Wang, X., Zheng, J., Wang, Y. and Zhu, Y. (2015). miR-381 regulates neural stem cell proliferation and differentiation via regulating Hes1 expression. *PLoS ONE.* **10**, e0138973. doi:10.1371/journal.pone.0138973

Shimojo, H., Ohtsuka, T. and Kageyama, R. (2008). Oscillations in notch signaling regulate maintenance of neural progenitors. *Neuron* **58**, 52-64. doi:10.1016/j.neuron.2008.02.014

Shitamukai, A., Konno, D. and Matsuzaki, F. (2011). Oblique radial glial divisions in the developing mouse neocortex induce self-renewing progenitors outside the germinal zone that resemble primate outer subventricular zone progenitors. *J. Neurosci.* **31**, 3683-3695. doi:10.1523/JNEUROSCI.4773-10.2011

Sueda, R., Imayoshi, I., Harima, Y. and Kageyama, R. (2019). High Hes1 expression and resultant Ascl1 suppression regulate quiescent vs. active neural stem cells in the adult mouse brain. *Genes Dev.* **33**, 511-523. doi:10.1101/gad.323196.118

Takahashi, T., Nowakowski, R. S. and Caviness, V. S.Jr. (1995). The cell cycle of the pseudostratified ventricular epithelium of the embryonic murine cerebral wall. *J. Neurosci.* **15**, 6046-6057. doi:10.1523/JNEUROSCI.15-09-06046.1995

Takahashi, T., Goto, T., Miyama, S., Nowakowski, R. S. and Caviness, V. S., Jr. (1999). Sequence of neuron origin and neocortical laminar fate: relation to cell cycle of origin in the developing murine cerebral wall. *J. Neurosci.* **19**, 10357-10371. doi:10.1523/JNEUROSCI.19-23-10357.1999

Tan, S. L., Nishi, M., Ohtsuka, T., Matsui, T., Takemoto, K., Kamio-Miura, A., Aburatani, H., Shinkai, Y. and Kageyama, R. (2012). Essential roles of the histone methyltransferase ESET in the epigenetic control of neural progenitor cells during development. *Development* **139**, 3806-3816. doi:10.1242/dev.082198

Tarabykin, V., Stoykova, A., Usman, N. and Gruss, P. (2001). Cortical upper layer neurons derive from the subventricular zone as indicated by Svet1 gene expression. *Development* **128**, 1983-1993.

Development (2021) 148, dev189191. doi:10.1242/dev.189191

Wang, X., Tsai, J.-W., LaMonica, B. and Kriegstein, A. R. (2011). A new subtype of progenitor cell in the mouse embryonic neocortex. *Nat. Neurosci.* **14**, 555-561. doi:10.1038/nn.2807

Watanabe, N., Kageyama, R. and Ohtsuka, T. (2015). Hbp1 regulates the timing of neuronal differentiation during cortical development by controlling cell cycle progression. *Development* **142**, 2278-2290. doi:10.1242/dev.120477

Figure S1 Ohtsuka et al.

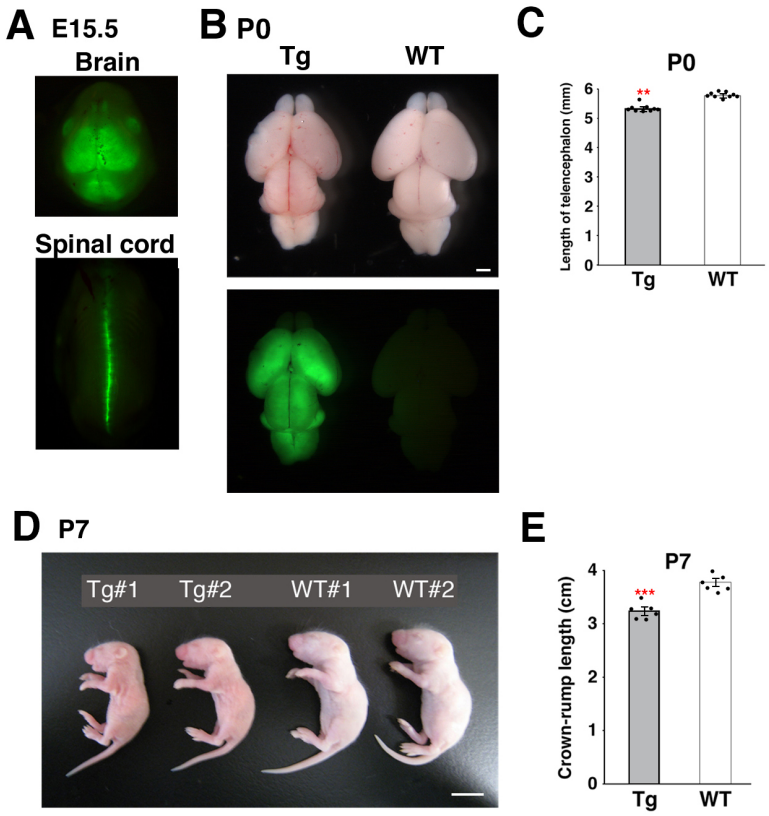

Fig. S1. Appearance of Hes1-overexpressing Tg mice and GFP expression in the central nervous system. (**A**) GFP expression in the brain and spinal cord of Tg mice at E15.5. (**B**) Appearance of Tg and WT brains and GFP expression at P0. (**C**) Comparison of the length of telencephalon of Tg vs WT pups at P0. (**D**) Appearance of the whole body of Tg and WT mice at P7. Note that the Tg pups exhibit smaller body size. (**E**) Comparison of body size (crown-rump length) of Tg vs WT pups at P7. Data are presented as mean±s.e.m. (n=9 for C; n=6 for E); **P<0.01, ***P<0.001 (Student's t-test). Scale bars: 1 mm in B; 10 mm in D.

Figure S2 Ohtsuka et al.

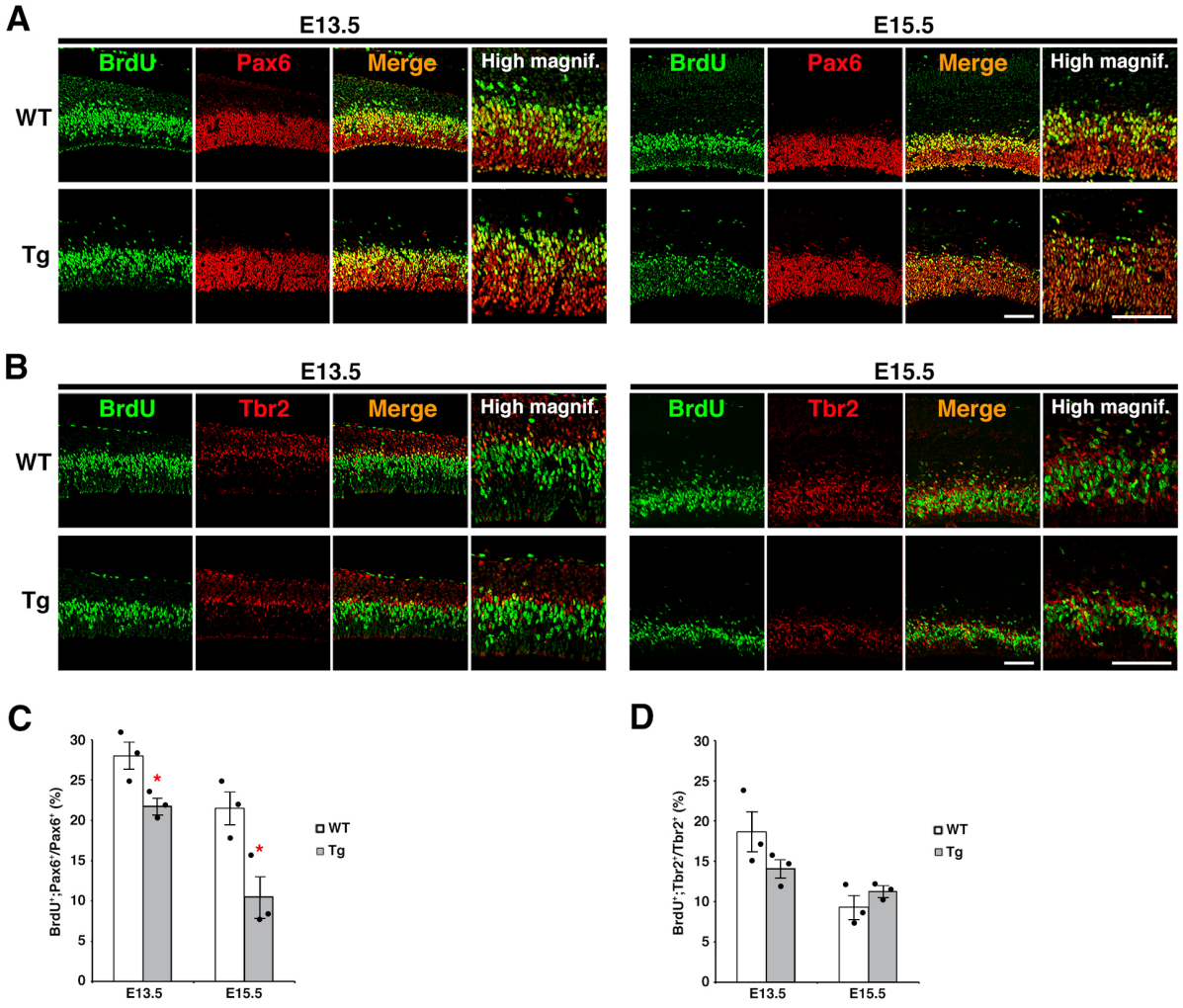

Fig. S2. Cell proliferation rate in NSCs and IPCs. (**A,B**) Double-labeling with anti-BrdU (green) and anti-Pax6 (red) (A) or anti-Tbr2 (red) (B) antibodies on coronal sections of neocortical regions of WT and Tg mice at E13.5 and E15.5. BrdU was injected intraperitoneally into pregnant mice 30 minutes before sacrifice. Higher magnification views are shown in the right panels. (**C,D**) Graphs showing the proportions of $BrdU^+$ cells among $Pax6^+$ cells (C) or $Tbr2^+$ cells (D). Data are presented as mean±s.e.m. (n=3); *P<0.05 (Student's t-test). Scale bars: 100 µm.

Figure S3 Ohtsuka et al.

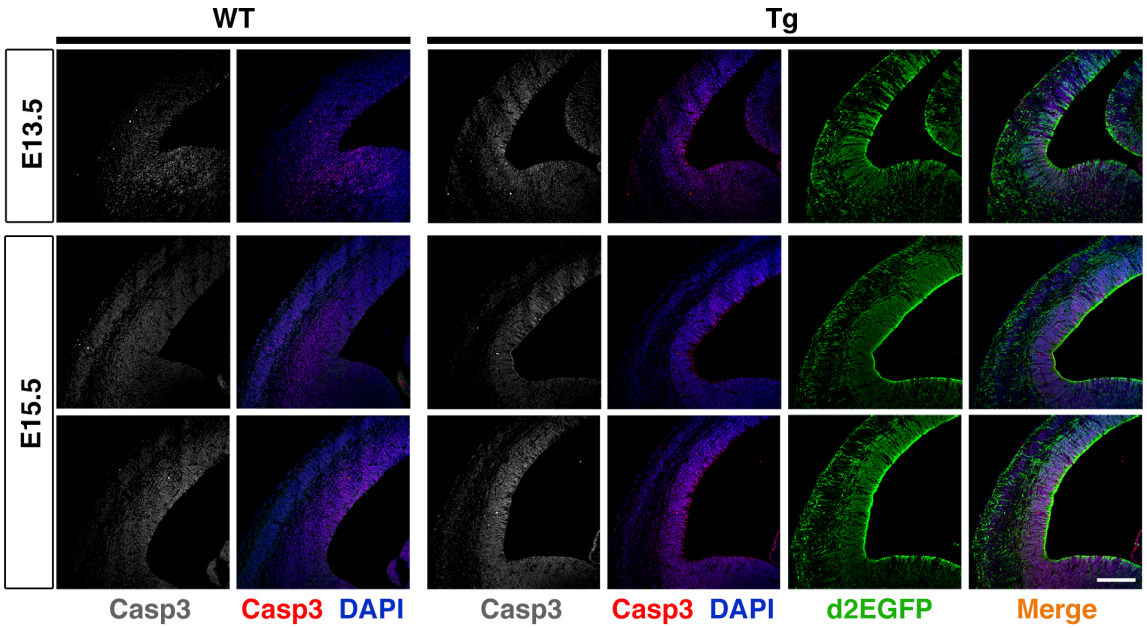

Fig. S3. Estimation of cell death in embryonic neocortical regions. Coronal sections of neocortical regions of WT and Tg embryos at E13.5 and E15.5 were immunostained with anti-cleaved caspase-3 (Casp3) (red) and anti-GFP (green) antibodies. Casp3 signals are shown in white on the left panels (grey scale). DAPI (blue) represents nuclear staining. Scale bars: 200 μm.

Figure S4 Ohtsuka et al.

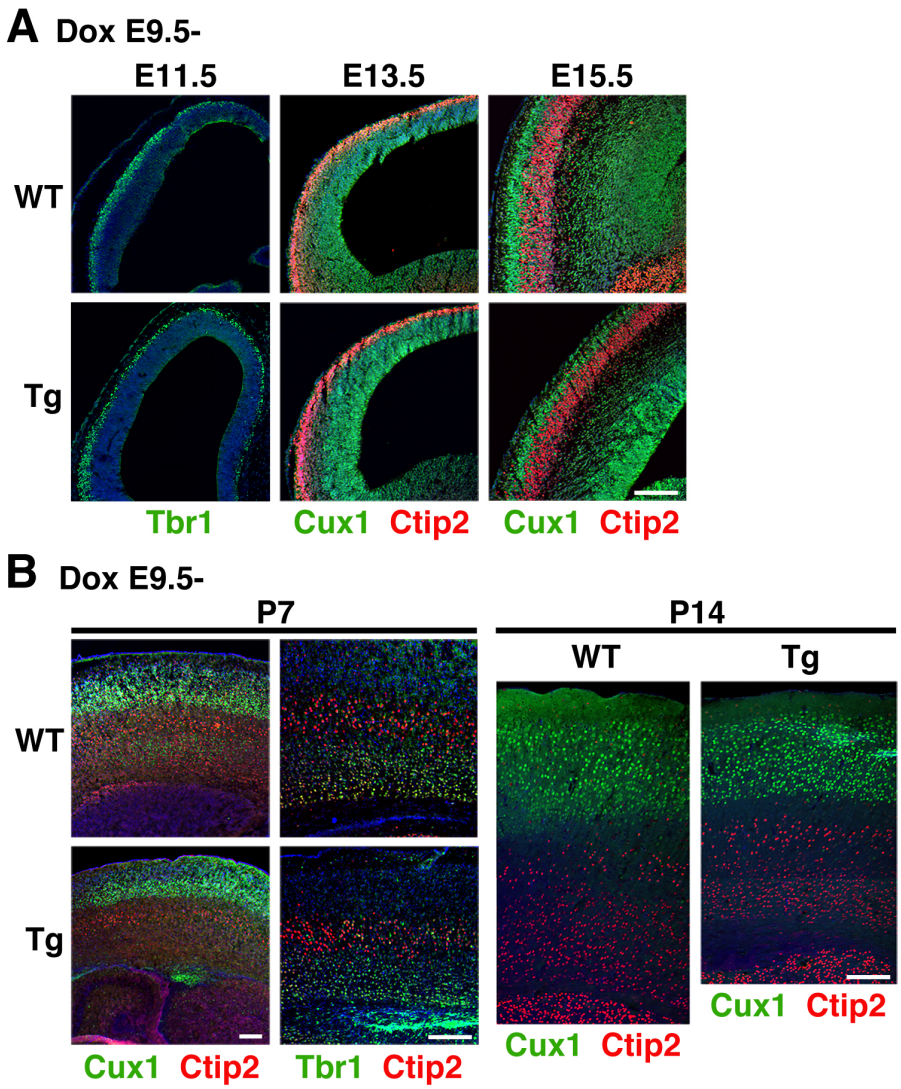

Fig. S4. Neurogenesis at early to mid-embryonic stages and layer structure of the postnatal cerebral cortex. (**A**) Immunohistochemistry on coronal sections of the dorsolateral telencephalon of WT and Tg embryos; immunostaining with an anti-Tbr1 (green) antibody at E11.5 and double-labeling with anti-Cux1 (green) and anti-Ctip2 (red) antibodies at E13.5 and E15.5. (**B**) Immunohistochemistry on coronal sections of WT and Tg cortices with anti-Cux1 (green), anti-Ctip2 (red), and anti-Tbr1 (green) antibodies at P7; and with anti-Cux1 (green) and anti-Ctip2 (red) antibodies at P14. Scale bars: 200 μm.

Figure S5 Ohtsuka et al.

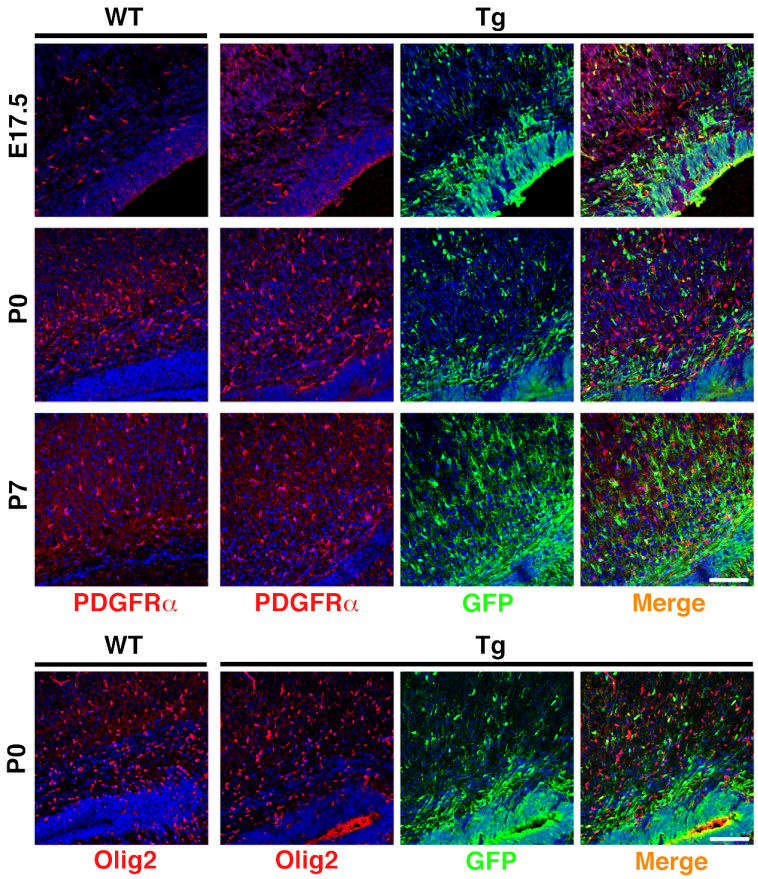

Fig. S5. Analysis of generation of oligodendrocyte lineage. Immunohistochemistry on coronal sections of neocortical regions of WT and Tg brains; immunostaining with anti-GFP (green) and anti-PDGFRα (red) antibodies at E17.5, P0, and P7; and with anti-GFP (green) and anti-Olig2 (red) antibodies at P0. DAPI (blue) represents nuclear staining. Scale bars: 100 μm.

Figure S6 Ohtsuka et al.

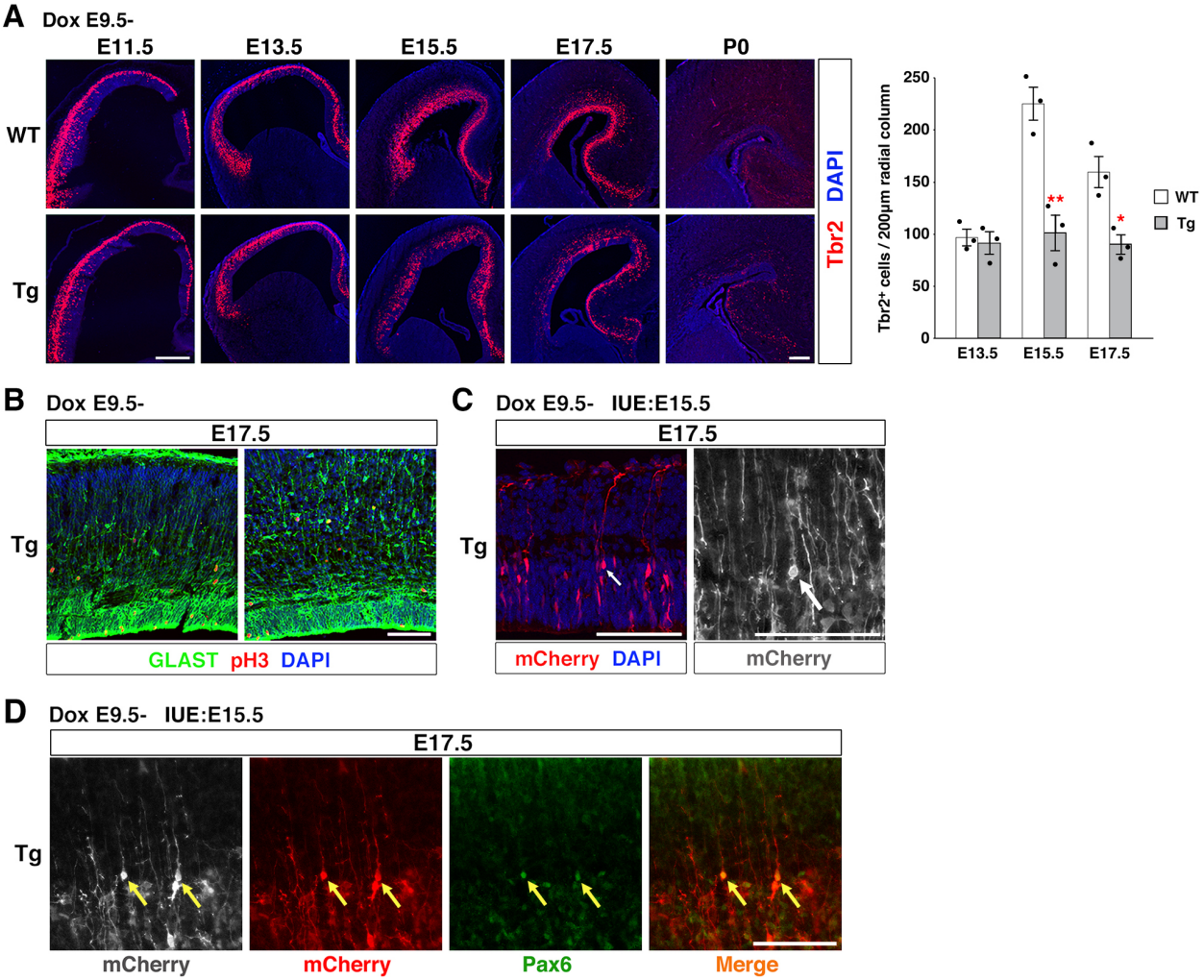

Fig. S6. Decrease in Tbr2$^+$ IPCs and increase in bRGC-like cells. (**A**) Immunostaining with anti-Tbr2 (red) antibody on coronal sections of the dorsal telencephalon of WT and Tg mice at various developmental stages. (**B**) Double-labeling with anti-GLAST (green) and anti-pH3 (red) antibodies on coronal sections of neocortical regions of E17.5 Tg embryos. (**C,D**) *pEF-mCherry* expression vectors were transfected into the VZ cells of Tg embryos by *in utero* electroporation (IUE) at E15.5. The morphology of transfected cells was analyzed by immunohistochemistry on coronal sections of neocortical regions at E17.5. (C) Single labeling with anti-mCherry antibody (red) with DAPI staining (blue). mCherry signals are shown in white on the right panel (grey scale). (D) Double labeling with anti-mCherry (red) and anti-Pax6 (green) antibodies. mCherry signals are shown in white on the left panel (grey scale). The arrows indicate mCherry$^+$ cells with bRGC-like morphology that retain only basal radial processes but lack apical processes and are located in the SVZ. The yellow arrows in (D) indicate mCherry$^+$;Pax6$^+$ cells in the SVZ. DAPI (blue) represents nuclear staining. Data are presented as mean±s.e.m. (n=3); *P<0.05, **P<0.01 (Student's t-test). Scale bars: 200 μm in A; 100 μm in B, C, D.

Figure S7 Ohtsuka et al.

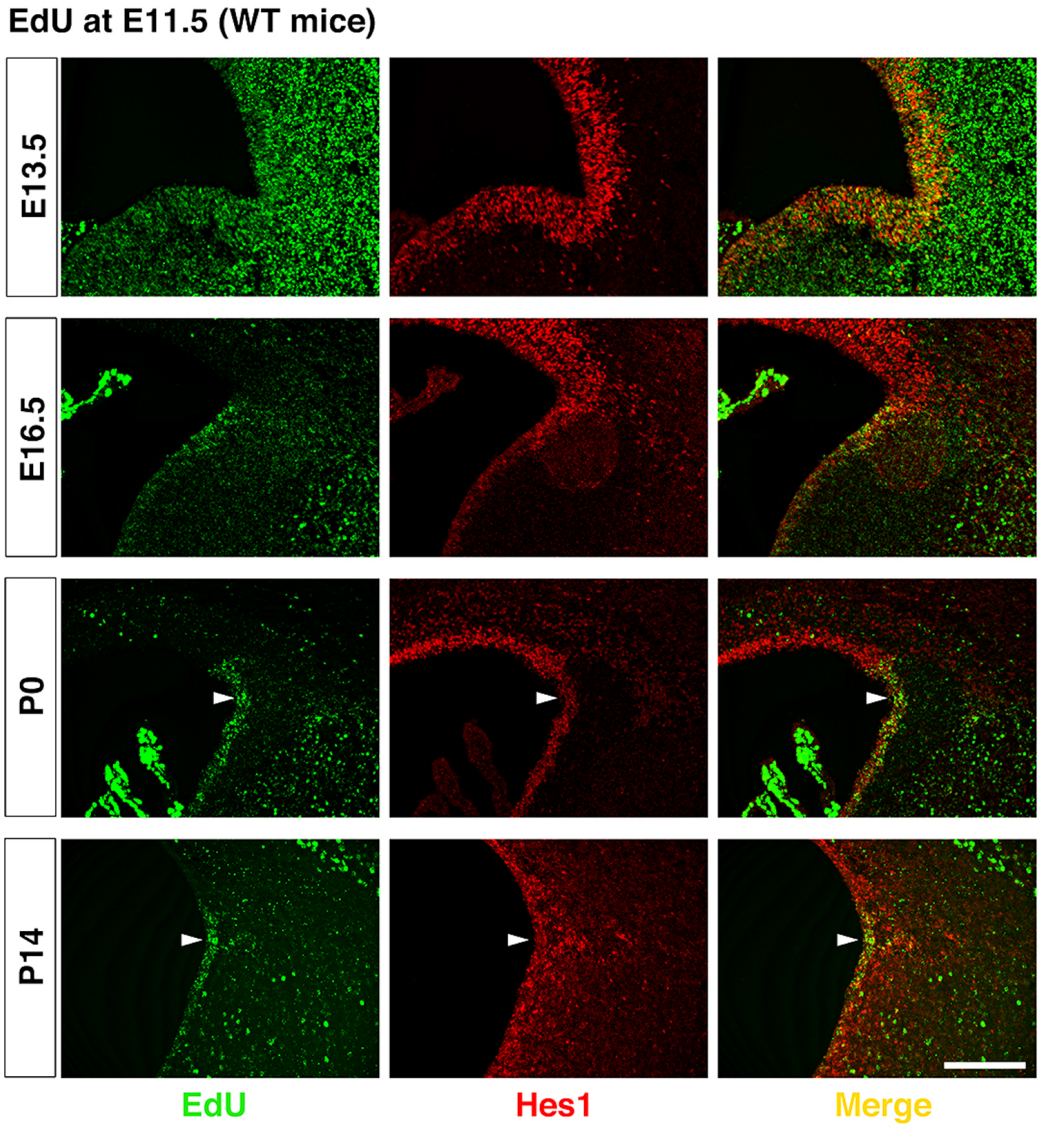

Fig. S7. Estimation of Hes1 expression levels in EdU label-retaining cells in the SVZ. EdU was injected intraperitoneally into WT pregnant mice at E11.5 and detected by Click reaction at E13.5, E16.5, P0 and P14 using Alexa Fluor 488 Azide (green). In addition, immunostaining with anti-Hes1 antibody (red) was performed on coronal brain sections. EdU label-retaining cells were observed in the SVZ around the dorso-ventral boundary and the ventrolateral wall of lateral ventricles. Note that Hes1 expression levels in these EdU label-retaining cells (white arrowheads) were equivalent to or rather lower than those in surrounding EdU^- cells in the SVZ at postnatal stages. Scale bar: 200 μm.

Table S1. Primary antibodies

Antigen	Host	Manufacturer	Catalogue No.	Dilution
GFP	rabbit	Molecular Probes	A11122	1:500
GFP	chicken	Abcam	Ab13970	1:500
Hes1	rabbit	Kobayashi et al., 2009	----------	1:1000
Tuj1	mouse	Covance	MMS-435P	1:1000
Pax6	rabbit	Covance	PRB-278P	1:200
Brn-1	goat	Santa Cruz	sc-6028	1:100
Neurog2	goat	Santa Cruz	sc-19223	1:1000
BrdU	mouse	Becton Dickinson	347580	1:100
BrdU	rat	Serotec	MCA2060	1:500
pH3	mouse	Sigma-Aldrich	H6409	1:500
Ki67	mouse	BD Pharmingen	556003	1:100
Ccnd1	rabbit	Thermo Scientific	RM-9104-SO	1:100
Cux1	rabbit	Santa Cruz	sc-13024	1:100
Ctip2	rat	Abcam	ab18465	1:500
GFAP	rabbit	DAKO	Z0334	1:500
NeuN	mouse	Merck Millipore	MAB337	1:500
Tbr2	rabbit	Abcam	ab23345	1:500
Tbr2	rat	eBioscience	14-4875-82	1:500
pVim	mouse	MBL International	D076-3S	1:500
mCherry	rat	Life technologies	M11217	1:500
Dcx	goat	Santa Cruz	sc-8066	1:200
Cleaved Caspase-3	rabbit	Cell Signaling	#9661S	1:500
Tbr1	rabbit	Abcam	Ab31940	1:400
PDGFRα	rat	BD Pharmingen	558774	1:500
GLAST	guinea pig	Merck Millipore	AB1783	1:100

Reference:

Kobayashi, T., Mizuno, H., Imayoshi, I., Furusawa, C., Shirahige, K. and Kageyama, R. (2009). The cyclic gene Hes1 contributes to diverse differentiation responses of embryonic stem cells. *Genes Dev*. 23, 1870-1875.

Table S2. Primers for quantitative real-time RT-PCR

Gene	Primer	Sequence
Hes1	Fw (Forward)	5′-GTGAAGCACCTCCGGAACCTGCAGC-3′
	Rv (Reverse)	5′-GCGGGTCACCTCGTTCATGCACTCG-3′
Ccnd1	Fw	5′-TTGACTGCCGAGAAGTTGTGC-3′
	Rv	5′-TTGTTCTCATCCGCCTCTGGC-3′
Gapdh	Fw	5′-TGGGTGTGAACCACGA-3′
	Rv	5′-AAGTTGTCATGGATGACCTT-3′

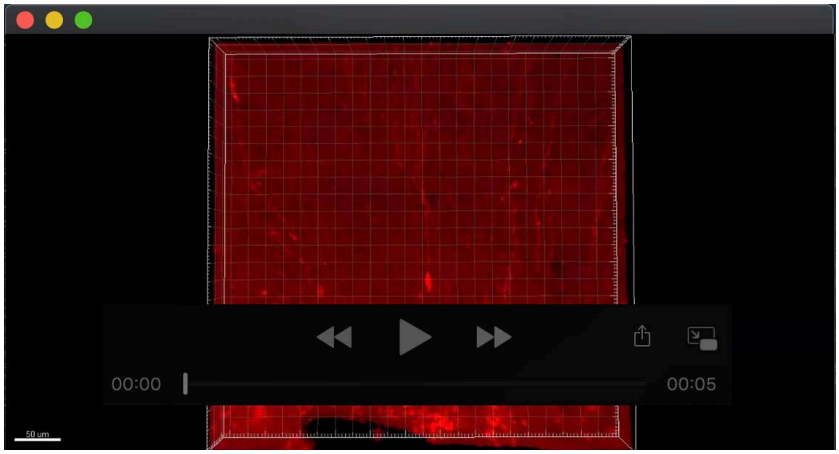

Movie 1. 3D image of bRGC-like cell

pEF-mCherry expression vectors were transfected into the VZ cells of Tg embryos by *in utero* electroporation at E15.5. Fixed and cryoprotected brain was cryosectioned at 70 µm and the morphology of transfected cells was analyzed by immunohistochemistry with anti-mCherry (red) antibody on a coronal section of neocortical region at E17.5. Note that a cell shown near the center of this movie exhibits a bRGC-like morphology that retains only basal radial processes but lacks apical processes and is located in the SVZ.